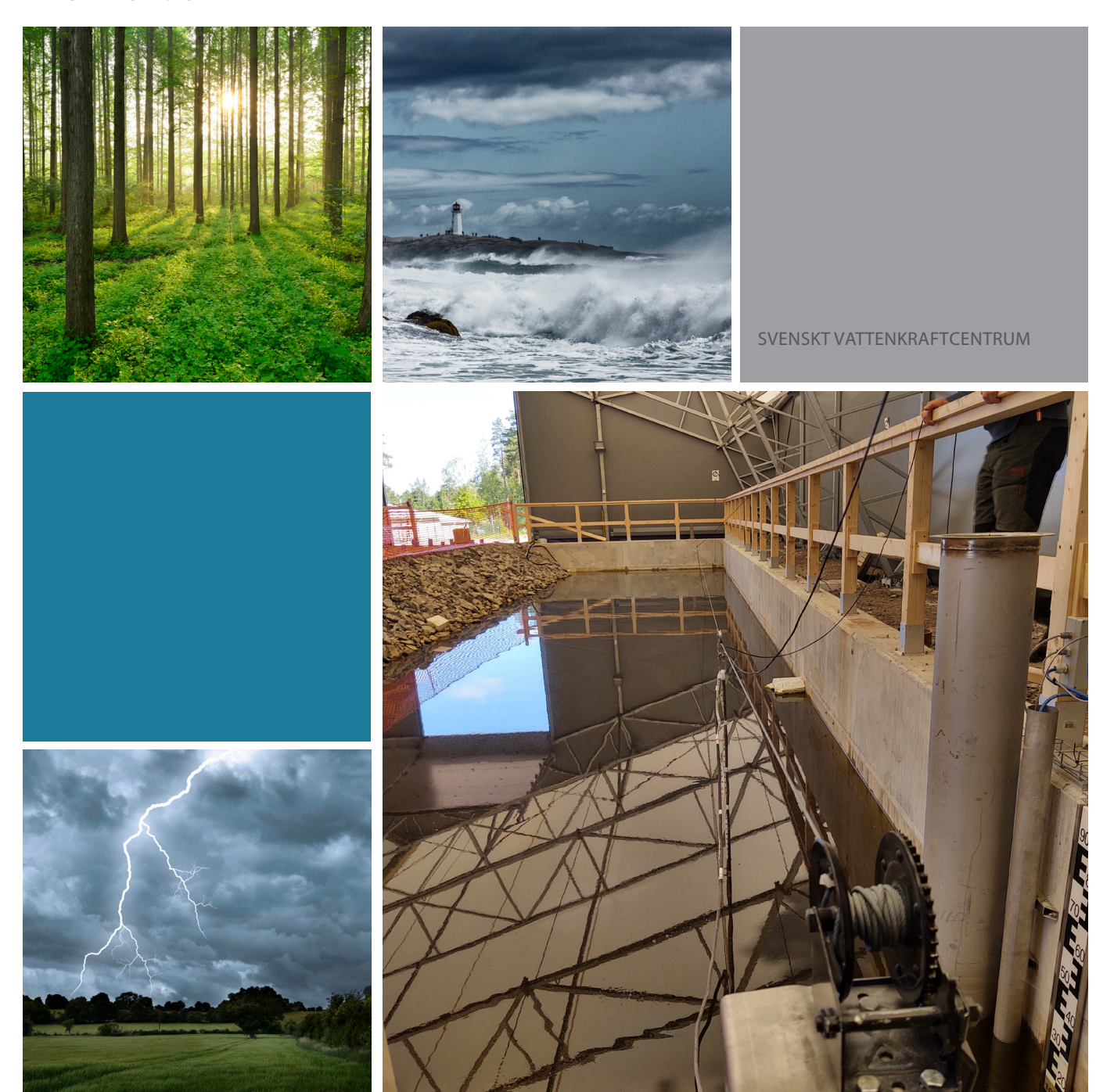
SEISMIC INVESTIGATIONS AT THE VATTENFALL EXPERIMENTAL DAM, ÄLVKARLEBY, SWEDEN: STAGE 2

REPORT 2024:1042





SEISMIC INVESTIGATIONS AT THE VATTENFALL EXPERIMENTAL DAM, ÄLVKARLEBY, SWEDEN: STAGE 2

CHRISTOPHER JUHLIN, SILVIA SALAS-ROMERO MONIKA IVANDIC, EMIL LUNDBERG

Foreword

This report outlines the work conducted from January 2021 to August 2022 (Stage 2) on seismic monitoring of the Vattenfall experimental dam at Älvkarleby. Building on previous efforts, this stage aimed to improve defect detection methods using advanced seismic techniques.

While the embedded defects were not directly detected, the project provided valuable insights into seismic monitoring, suggesting that time-lapse methods could enhance defect detection. These findings are important for the hydro industry, as they contribute to the development of techniques that help ensure dam safety.

The project Seismic investigations and monitoring of Vattenfall's experimental dam at Älvkarleby - project VKU14135 - was carried out in SVC – Swedish hydropower center.



Summary

This report provides an overview of work performed from January 2021 to August 2022 (Stage 2) in conjunction with the seismic component for detecting defects in the Vattenfall experimental dam at Älvkarleby. It is a continuation of the first stage of the project that involved experiments at the dam from November 2019 to December 2020. The experimental dam was equipped with five seismic cables inside it, each containing 24 hydrophones spaced at 0.8 m, giving a total 120 hydrophone pressure sensors. An array of 25 source boreholes, about 0.5-0.6 m deep along the crest, were also built into the dam for allowing borehole sources to generate seismic waves. In addition, four deeper boreholes, extending to the base of the dam, were built into the structure to provide better geometries for measurement of the seismic velocities of the dam materials. A P-wave sparker source was mainly used in the boreholes, but S-wave sources were also used, particularly in the deeper boreholes. During Stage 1 a cable was installed on the upstream side of the dam to allow the sparker source to be activated in the water in the reservoir. This greatly increased in the frequency range of the signals that could be recorded, up to 5000 Hz. An additional cable closer to the dam crest was installed during Stage 2. However, data recorded with the source activated along this cable did not add significant information.

Data were acquired in 6 campaigns during the period November 2019 to December 2020 in Stage 1. Two additional acquisition campaigns were carried out in Stage 2, one in May and the other starting in late June and extending into the first day of July. Extensive analyses of the data have been performed in which changes in the characteristics of the recorded data over the eight campaigns are documented in this report. An important observation is that the amplitude and frequency content of the seismic waves generated by the source in the boreholes and in the reservoir increases throughout the observation period. This suggests that full saturation of the dam (in a seismic sense) was not reached during the period of the observations. This has implications for the repeatability of the measurements, but also for the capability of detecting defects. None of the six built-in defects could be detected. In order to better understand the reason for not detecting any defects in spite of the high frequencies generated when shooting in the reservoir the seismic response from the six defects has been modeled in 3D using a relatively realistic velocity model. For only one of the defects is there a clear response from the defect. This is attributed to internal reflections within the model and from the sides of the dam masking the diffraction response of the other defects. However, when a baseline response is subtracted that was generated from a model with no defects then the signature of the defects become apparent. This suggests that time lapse monitoring of a dam may be an option for detecting defects that develop with time.

Even though no defects were detected valuable experience has been gained in applying seismic methods to dam monitoring. As a next step it is suggested that



distributed acoustic sensing (DAS) be tested on a real dam where fiber optic cables are already installed to determine if the high frequencies recorded at Älvkarleby can also be recorded on such a sensor. Other objectives would be to better test the repeatability of the source and determine velocities within the real dam by recording along the entire fiber optic layout.

Keywords: Seismic imaging, P-waves, seismic source, seismic modeling, amplitude, frequency, borehole



Sammanfattning

Denna rapport ger en översikt över arbete som utförts från januari 2021 till augusti 2022 (Stage 2) i samband med den seismiska komponenten för att upptäcka defekter i Vattenfalls försöksdammen i Älvkarleby. Det är en fortsättning på den första etappen av projektet som involverade experiment vid dammen från november 2019 till december 2020. Experimentdammen var utrustad med fem seismiska kablar inuti den, som var och en innehöll 24 hydrofoner med 0,8 m emellan de, vilket ger totalt 120 trycksensorer. En uppsättning av 25 källborrhål, cirka 0,5-0,6 m djupa längs krönet, byggdes också in i dammen för att tillåta borrhålskällor att generera seismiska vågor. Dessutom byggdes fyra djupare borrhål in ner till dammens botten för att ge bättre geometrier för mätning av dammmaterialens seismiska hastigheter. En P-vågs gnistkälla användes huvudsakligen i borrhålen, men även S-vågskällor användes, särskilt i de djupare borrhålen. Under Stage 1 installerades en kabel på uppströmssidan av dammen för att möjliggöra att gnistkällan kunde aktiveras i vattnet i reservoaren. Detta ökade kraftigt frekvensområdet för de signaler som kunde spelas in, upp till 5000 Hz. En extra kabel närmare krönet installerades under Stage 2. Data som registrerats med källan aktiverad längs denna kabel tillförde dock ingen signifikant information.

Data samlades in i 6 kampanjer under perioden november 2019 till december 2020 i Stage 1. Ytterligare två kampanjer genomfördes i Stage 2, en i maj och den andra med start i slutet av juni och som sträckte sig in i den första dagen i juli. Omfattande analyser av data har utförts där förändringar i egenskaperna hos de registrerade data under de åtta kampanjerna dokumenteras i denna rapport. En viktig observation är att amplitud- och frekvensinnehållet i de seismiska vågorna som genereras av källan i borrhålen och i reservoaren ökar under observationsperioden. Detta tyder på att full mättnad av dammen (i seismisk mening) inte uppnåddes under observationsperioden. Detta har konsekvenser för mätningarnas repeterbarhet, men också för förmågan att upptäcka defekter. Ingen av de sex inbyggda defekterna kunde upptäckas. För att bättre förstå orsaken till att inga defekter upptäcktes trots de höga frekvenser som genererades vid skjutning i reservoaren har den seismiska responsen från de sex defekterna modellerats i 3D med en relativt realistisk hastighetsmodell. För endast en av defekterna finns det en tydlig respons från defekten. Detta beror sannolikt på inre reflektioner inom modellen och från dammens sidor maskerar diffraktionsresponsen av de andra defekterna. Men när baslinjeresponsen subtraheras, genererat från en modell utan defekter, blir signaturerna från defekterna uppenbara. Detta tyder på att tidsförloppsövervakning av en damm kan vara ett alternativ för att upptäcka defekter som utvecklas med tiden.

Även om inga defekter upptäcktes har värdefulla erfarenheter erhållits I dessa studier. Som nästa steg föreslås att distribuerad akustisk avkänning (DAS) testas



på en riktig damm där fiberoptiska kablar redan är installerade för att avgöra om de höga frekvenserna som registrerats vid Älvkarleby också kan registreras på en sådan sensor. Andra mål skulle vara att bättre testa källans repeterbarhet och bestämma hastigheter inom den verkliga dammen genom att registrera signaler längs hela den fiberoptiska layouten.



List of content

1	Introduction				
	1.1	Background	9		
	1.2	The Älvkarleby experimental dam	9		
	1.3	Purpose of this report	10		
2	Seismic data acquisition				
	2.1	Overview of dam geometry	11		
	2.2	Instrumentation	11		
	2.3	Recording campaigns	12		
	2.4	A note on seicmic wave propagation in loose sediments	14		
3	Data analysis				
	3.1	Source on the crest of the dam	15		
	3.2	Source in deep boreholes	20		
	3.3	Source in the reservoir	20		
	3.4	Amplitude observations	24		
	3.5	Identification of first arrivals for velocity determination	29		
	3.6	Estimates of $V_{\text{\tiny P}}$ and $V_{\text{\tiny S}}$ velocities and possible changes with time	35		
4	Data evaluation				
	4.1	Potential defects	36		
	4.2	Seismic modeling	36		
	4.3	Outlook	41		
5	Conc	lusions	45		
6	Refe	rences	46		



1 Introduction

1.1 BACKGROUND

Embankment dams are the most common type of dam worldwide (Deangeli et al. 2009). These structures act as water barriers and are classified as earth fill and rock fill dams depending on the amount of natural materials (soil and rock) used in their construction. There are different classes depending on the position of the core, filter, drainage, transition and facing zones. The purpose of these zones is to avoid the loss of soil particles by water seepage (internal erosion and piping), and decrease pore water pressure and the leakage caused by seepage flow through the embankment (Deangeli et al. 2009).

Embankment dam failures are mostly related to overtopping or seepage, and can have devastating effects on the economy and environment, as well as loss of human lives (Deangeli et al. 2009; Sharma and Kumar 2013). Failures occur in a great number of cases during the first filling or within five years of the construction of the dam (Sharma and Kumar 2013).

Deterioration of the body and foundation of these structures may also develop progressively along the years of the 'service life'. For example, in the case of Sweden, 60% of the large embankment dams built before 1997 have suffered deterioration to some degree (Norstedt and Nilsson 1997). Increase in outflows and erosion rate may be related to preferential flow directions created by cavities, channels and fracture zones (Kayode et al. 2018). The difficulty in detecting and mapping these damages can be overcome by combining invasive (borehole data) and non-invasive (geophysical data such as resistivity and temperature) investigation techniques, achieving higher lateral resolution and reducing uncertainties (Woolery 2018).

Some examples (Adamo et al. 2020; Ikard et al. 2014; Kim et al. 2007) of non-invasive, cost-effective indirect geophysical methods for evaluating the conditions within embankment dams are: self-potential (sensitive to seepage flows), electromagnetics (sensitive to saturation, porosity and temperature), electric resistivity tomography (sensitive to saturation, porosity and fluid content), ground penetrating radar (sensitive to buried man-made objects, groundwater and soil/rock interfaces), reflection seismic (sensitive to sinkholes, bedrock interface), magnetics (buried man-made objects), gravity (cavities), and temperature (paths by establishing hydraulic connections). Thus, the information obtained in geophysical surveys can contribute to monitoring for failure and assessing the dam's structural integrity.

1.2 THE ÄLVKARLEBY EXPERIMENTAL DAM

Vattenfall initiated a research project to assess the potential of geophysical methods for detecting a number of purpose-built defects within the core of a dam and to monitor the dam's behavior using geotechnical instrumentation. The project has been carried out in an experimental dam built in Älvkarleby (Sweden), where defects of unknown position and size were built-in within its core. Various sets of



geophysical instrumentation were installed in the dam in 2019 (hydrophones, electrodes and optical fiber for performing seismic, resistivity, temperature and acoustic sensing measurements), as well as geotechnical equipment (inclinometers, piezometers for pore water pressure and strain measurements). Uppsala University has been responsible for the seismic measurements and data analyses within Stage 1 were performed in the time period October 2019 to December 2020 (Salas-Romero et al., 2021). Seismic data were acquired in 6 campaigns during this phase with the aim of evaluating the potential of seismic methods for detecting the built-in defects. In spite of a significant processing effort it was not possible to say with certainty the position of any of the defects.

1.3 PURPOSE OF THIS REPORT

Initially the locations of the defects were to be revealed at the end of 2020, but delays in filling of the dam and requests for additional measurement time from others involved in the project resulted in the locations being revealed first in June 2022 (Lagerlund et al., 2022). Uppsala University therefore requested additional funds from SVC to acquire additional seismic data in two campaigns and to continue to analyze the existing data. Main objectives of this 2nd study were:

- Continue trying to localize the defects through data processing
- Gain an improved understanding of the seismic response of the dam with time through analysis of changes in seismic velocity and frequency content of the data
- Perform a post-mortem on the seismic data once the location of the defects were known to determine if there are signs of them in the data that could have been missed.

First, we present an overview of the seismic data acquisition, before presenting results from the data analysis. For detailed information on the seismic processing performed to locate the defects the reader is referred to the Stage 1 report by Salas-Romero et al. (2021). Extensive 3D seismic modeling has also been performed now to better understand the seismic response of the defects and the potential to detect them. Finally, we present an outlook on how to best proceed in developing high resolution seismic methods for dam monitoring.



2 Seismic data acquisition

2.1 OVERVIEW OF DAM GEOMETRY

The construction of the dam and the filling of the water reservoir took around two full months. The dam structure (see Figure 1) is 20 m long, 4 m high and 15 m wide at the bottom and was built within a concrete box (with fiberglass reinforcement at the base). It is composed of four types of material: the central part consists of an impermeable core (A–clay) about 3.5 m high with a thickness of 1.6 m at the bottom and 1.1 m at the top. The core is surrounded by a fine filter (B–sand) 0.5-0.9 m wide on the sides and 0.1 m high on top. On each side of the fine-filter there are two walls of a coarse filter (C–gravel) approximately 0.5 m wide. Covering these materials, support filling (D–crushed stone) is present, extending up to 5.3 m at the bottom in both the upstream and downstream directions with a slope inclination of about 34 degrees.

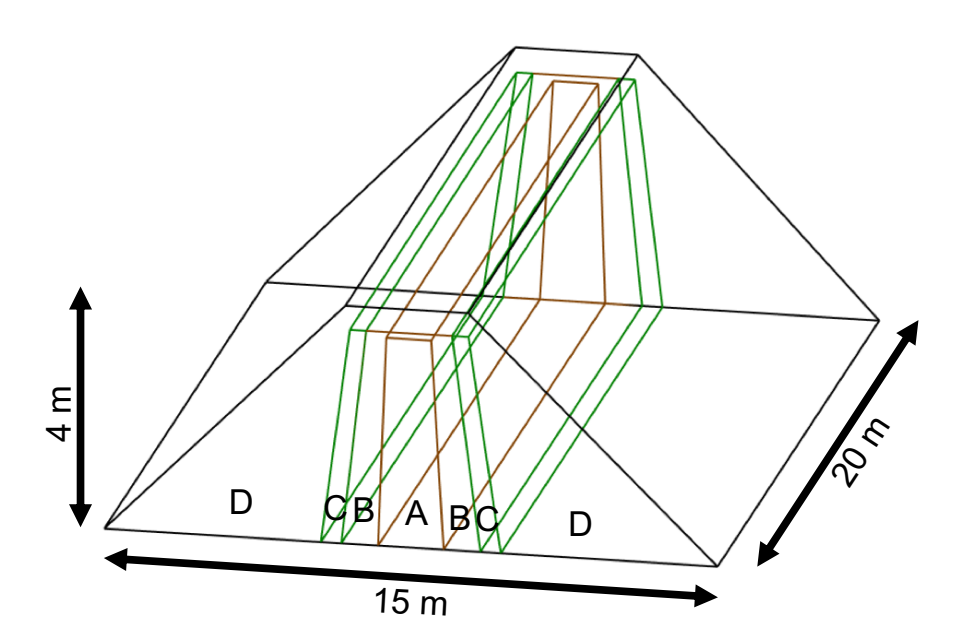


Figure 1. Dam geometry with four types of materials, A-clay (impermeable core), B-sand (fine filter), C-gravel (coarse filter), and D-crushed stone (support filling).

2.2 INSTRUMENTATION

The seismic acquisition equipment (see Figure 2) was composed of five lines of 24 hydrophones each. The length of each line was 18.4 m with hydrophones spaced at approximately 0.8 m. Three of the lines were installed close to the top of the dam's core and two at the bottom on each side of the core, i.e. none of the hydrophone lines were within the core. These lines were named depending on their position on the dam as 1000 (top middle), 2000 (top upstream), 3000 (top downstream), 4000 (bottom upstream), and 5000 (bottom downstream). The lines were powered by battery boxes (AA cells) on the surface, and their output connected to 24-channel seismographs (Geodes). The hydrophone sensors are characterized as being



sensitive to the frequency range 1-10000 Hz. Four deeper boreholes were also used for the seismic acquisition. A single 3-component geophone was used to record data in them while either a P-wave or S-wave borehole source was activated. For a description of the sources used see Salas-Romero et al. (2021).

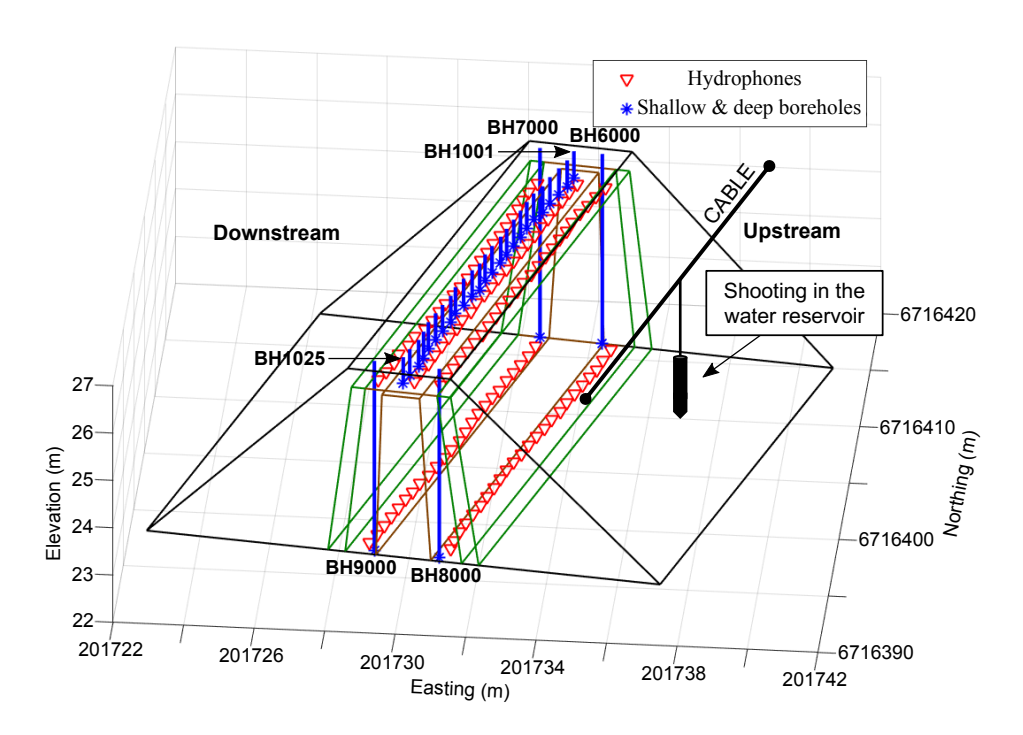


Figure 2. Overview of the installed seismic equipment (hydrophones), and shallow (BH1001 to BH1025) and deep (BH6000 to BH9000) boreholes where seismic sources were used.

2.3 RECORDING CAMPAIGNS

Eight seismic field campaigns were performed from November 2019 to June 2022 (Figure 3). The seismic data were generally acquired using five Geodeseismographs each recording 24 channels, and connected to a field laptop for collecting the data. The Geodes interconnection allowed recording up to a total of 120 channels at the same time. Therefore, all hydrophone lines (120 hydrophones in total) could be recorded simultaneously or a combination of four hydrophone lines with the 3C-borehole geophone. The borehole seismic sources were positioned in the shallow and deep boreholes installed on the crest of the dam (Figure 2). The IPG5000 impulse generator was located inside the container located next to the dam (it had to be protected from water and dust, the same for the connections between the impulse generator and the seismic sources). Control and triggering of the seismic sources were done through a remote-control unit. Additionally, a cable was installed in the upstream side of the dam, above the water reservoir, for hanging the seismic source (Figure 2) and shooting at multiple positions along the cable. Passive data were also collected twice, in campaigns 5 and 6, over several days with recording on 24 (line 4000, October 2020) and 72 channels (lines 2000, 4000 and 5000, November-December 2020). In Stage 2 of the project an additional cable was installed across the dam that was closer to the crest.



	November 2019	February 2020	April 2020	June & July 2020	October 2020	November & December 2020	May 2021	June & July 2021
Reservoir saturation	•		Partial (reservoir full for 3 weeks)	Partial (reservoir full for 1 month)	"Fully saturated"	"Fully saturated"	"Fully saturated"	"Fully saturated"
			~2.7-3 m	~3.19-3.3 m	~3.17-3.19 m	~3.171 m	~3.171 m	~3.171 m
Survey param								
Receiver type	Hydrophone / 3C- borehole geophone	Hydrophone / 3C-borehole geophone	Hydrophone / 3C-borehole geophone	Hydrophone / 3C-borehole geophone	Hydrophone / 3C-borehole geophone	Hydrophone / 3C- borehole geophone	Hydrophone / 3C- borehole geophone	Hydrophone / 3C- borehole geophone
Recording hydrophone lines / boreholes	1000, 2000, 3000, 4000, & 5000 / BH6000 & BH7000	1000, 2000 & 3000 / BH7000	1000, 2000 & 4000 / BH6000, BH7000 & BH9000	1000, 2000, 3000, 4000, & 5000 / BH6000, BH7000 & BH8000	1000, 2000, 3000, 4000, & 5000 / BH6000, BH7000 & BH8000	1000, 2000, 3000, 4000, & 5000 / BH6000, BH7000 & BH9000	1000, 2000, 3000, 4000, & 5000 / BH6000, BH7000 & BH8000	1000, 2000, 3000, 4000, & 5000 / BH6000, BH7000 & BH8000
	120	72	72	96	120	120	120	120
Hydrophon e spacing	~ 0.8 m	~ 0.8 m	~ 0.8 m	~ 0.8 m	~ 0.8 m	~ 0.8 m	~ 0.8 m	~ 0.8 m
	0.5 m (8 sampling points per borehole)	0.4 m (9 sampling points per borehole)	0.4 m (9 sampling points per borehole)	0.4 m (9 sampling points per borehole)	0.4 m (9 sampling points per borehole)	0.4 m (9 sampling points per borehole)	1 m (1-3 sampling points per borehole)	1 m (1-3 sampling points per borehole)
Source type	SBS42 / CHE	SBS42 / BIS-SH / CHE	SBS42 / BIS-SH	SBS42 / BIS-SH	SBS42	SBS42 / CHE	SBS42 / CHE	SBS42 / CHE
	BH1001- BH1025 / BH8000 & BH9000	BH1001- BH1025 / BH9000	BH1001- BH1025 / BH8000 & BH9000	BH1001- BH1025 / BH6000, BH7000, BH8000 & BH9000	BH1001- BH1025 / BH6000, BH7000 & BH8000	BH1001- BH1025 / BH6000, BH7000 & BH8000	BH1001- BH1025 / BH9000, BH7000 & BH8000	BH1001- BH1025 / BH9000 & BH7000
Number of shots	72	70	170	1851	1130	1064	483	742
	0.8 m / ~0.56 m	0.8 m / ~0.56 m	0.8 m / ~0.56 m	0.8 m / ~0.56 m	0.8 m / ~0.56 m	0.8 m / ~0.56 m	0.8 m / ~0.56 m	0.8 m / ~0.56 m
Shot sampling within deep boreholes	1 m (4 sampling points per borehole)	0.8 m (4 sampling points per borehole)	0.8 m (4 sampling points per borehole)	0.8 m (4 sampling points per borehole)	0.8 m (4 sampling points per borehole)	0.8 m (4 sampling points per borehole)	0.1 m (31 sampling points per borehole)	0.1 m (31 sampling points per borehole)
Shot spacing in reservoir	-	-		~0.2 m (100 points)				
Recording parameters								
	0.11 s	0.125 s / 0.51 s (borehole)	0.51 s	0.51 s	0.51 s / 0.128 s (water reservoir)/ 4 s (passive)	0.51 s / 0.128 s (water reservoir)/ 4 s (passive)	0.51 s / 0.128 s (water reservoir)	0.51 s / 0.128 s (water reservoir)
Sampling rate	0.0625 ms	0.0625 ms / 0.25 ms (borehole)	0.25 ms	0.25 ms	0.25 ms / 0.0625 ms (water reservoir)	0.25 ms / 0.0625 ms (water reservoir) / 2 ms (passive)	0.25 ms / 0.0625 ms (water reservoir)	0.25 ms / 0.0625 ms (water reservoir)

Figure 3. Overview of the eight recording campaigns.



2.4 A NOTE ON SEICMIC WAVE PROPAGATION IN LOOSE SEDIMENTS

For solid rock, for example granite, it is relatively straightforward to calculate seismic velocities given a certain mineral composition. For loose sediments, this is more challenging since the velocity also depends on porosity, the type of fluid in the pore space and how the fluid is distributed within the pores. Figure 4 shows how the arrival time decreases and amplitude increases of an ultrasonic wave when a sample is fully saturated. The differences in both are significant when compared to a dry sample. Partially saturated samples have velocities in between the two extremes. Figure 5 shows an example of how the core velocity of the dam may change with degree of saturation based on a patchy saturation model (e. g. Kazemeini et al., 2010). In this model velocities are above 1000 m/s first when over 95% saturation is reached. The model demonstrates the difficulty that may exist for determining P-wave velocities in a real dam as saturation degree changes.

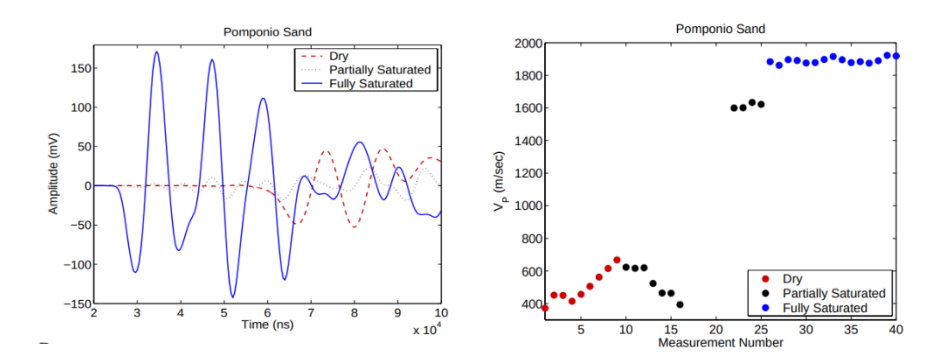


Figure 4. (Left) Waveforms recorded in ultrasonic experiments for different degrees of saturation. (Right) Ultrasonic velocities at different degrees of saturation. Figures from Zimmer (2003).

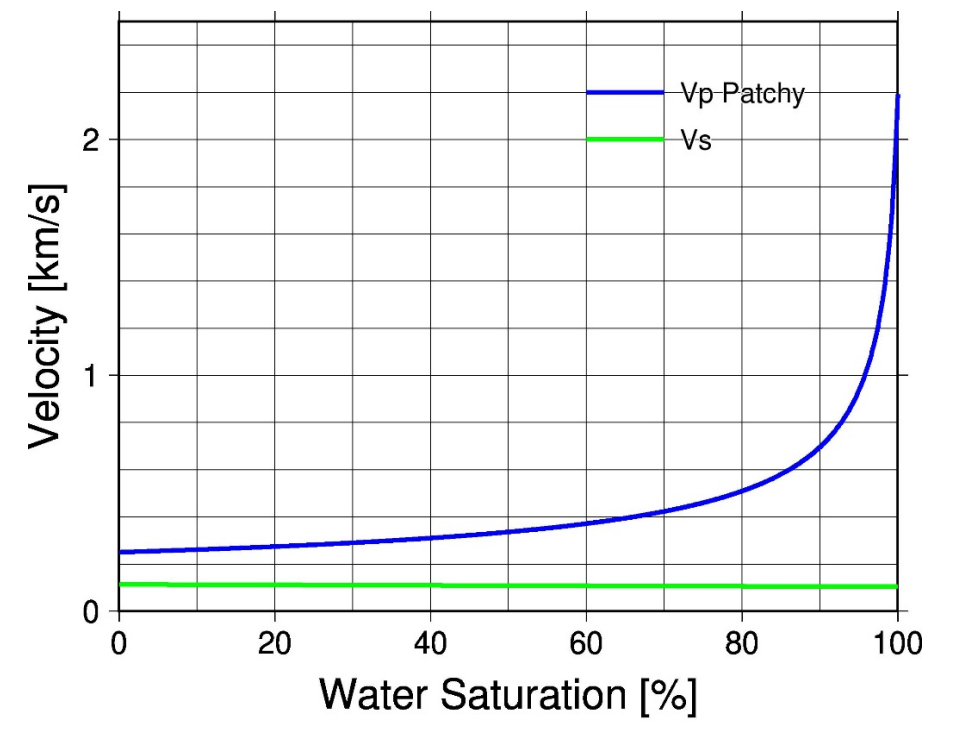


Figure 5. Seismic velocity as a function of saturation based on a patchy saturation model.



3 Data analysis

The various recording geometries allow the seismic response of different parts of the dam to be studied. In particular it is possible to observe changes in the seismic response of the dam as it becomes more saturated. In the following sections we present several examples of how the seismic response changes from selected acquisition geometries and in time.

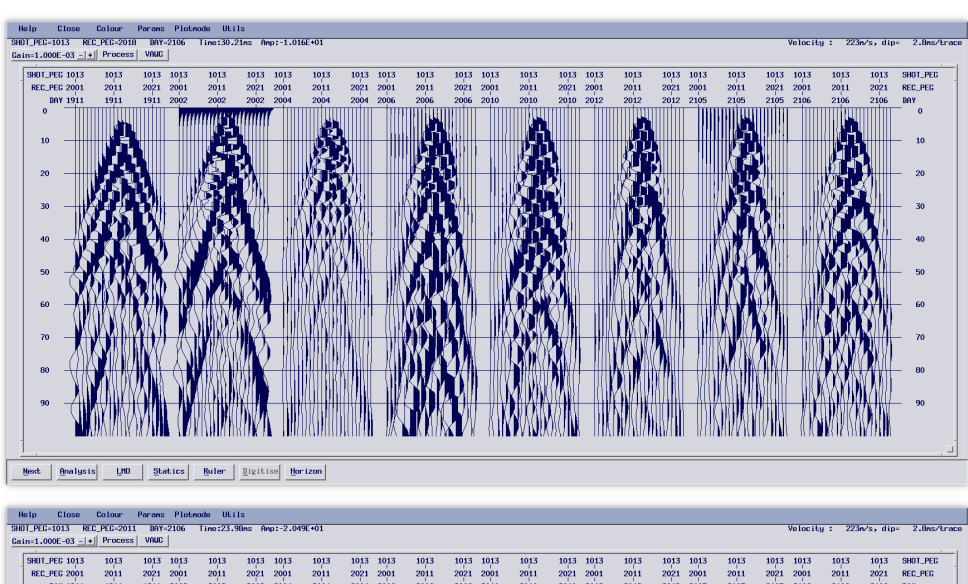
3.1 SOURCE ON THE CREST OF THE DAM

The P-wave source was activated in the boreholes on the crest of the dam for all surveys and hydrophone line 1000 recorded all of these. Figure 6 shows the seismic response without any processing for the source in borehole 1013, roughly in the center of the crest. The response is fairly similar for all campaigns, but with some variations in the amplitude of the signals and the timing of some of the arrivals. The difference in arrival times of the first breaks becomes more apparent when the data are corrected for linear moveout (the data are shifted corresponding to the source-receiver distance divided by a given velocity) using a velocity of 280 m/s. Velocities of the first arrival near the source point clearly decrease with time. For the last campaign the velocity of the first arriving waves is about 220 m/s. Figure 7 shows the same data as Figure 6, but with a bandpass filter of 400-800-5000-7000 Hz applied. This frequency band corresponds to the useful energy range for detecting flaws in the dam. The signal strength in this frequency range decreases with time. It is strongest in the first two campaigns, when the reservoir was empty. At larger offsets the first breaks arrive at a velocity of about 340 m/s. This corresponds to the velocity of air. On campaign 2002 (Feb 2020) a very clear reflection is observed with an apex at about 44 ms. The moveout of the reflection also corresponds to the velocity of air. This reflection is also observed in the other campaigns, but is weaker. An apex arrival time of 44 ms and normal moveout velocity of 340 m/s corresponds to a reflector located 7.5 m from line 1000. The upstream concrete wall is a good candidate for the structure generating this reflection. In the bottom panel of Figure 7 the data have been linear moveout corrected with a velocity of 340 m/s and trace amplitude balancing has been applied. The air wave energy seems to decrease in amplitude with time. In particular it is difficult to identify the air wave first arrival, but the reflection is still apparent. The first break velocities of 220-280 m/s at near offsets probably correspond to the unsaturated P-wave velocities of the support filling (crushed stone).

Figure 8 shows data recorded from source position 1013 on the crest into hydrophone line 4000 (bottom upstream). In this case first breaks on near offsets appear to arrive earlier as time progresses. In the middle panel different curves have been plotted corresponding to different velocities (red – 4200 m/s, blue – 1650 m/s, green – 420 m/s, yellow – 340 m/s) assuming direct waves through homogeneous media. On the raw data (top and middle panel in Figure 5) no clear arrivals corresponding to the blue curve can be observed. Most of the lower frequency energy arrives at a velocity corresponding to about 420 m/s with a tendency for this velocity to increase with time. In the frequency range 400-800-



5000-7000 Hz there is a clear trend for waves to arrive with a moveout pattern that parallels the blue curves, indicating they are propagating through a medium with an average velocity of 1650 m/s. The signal strength also becomes stronger with time. These waves are not observed for the 1911 and 2002 campaigns when there was no water in the reservoir. This velocity may represent the P-wave velocity of the saturated support filling or the filters. It is not clear what the lower frequency wave arriving at 420 m/s represents. For hydrophones located on the bottom downstream side the higher frequency arrivals are not observed (Figure 9), supporting the interpretation that the velocity of 1650 m/s corresponds to waves traveling through the saturated support filling on the upstream side.



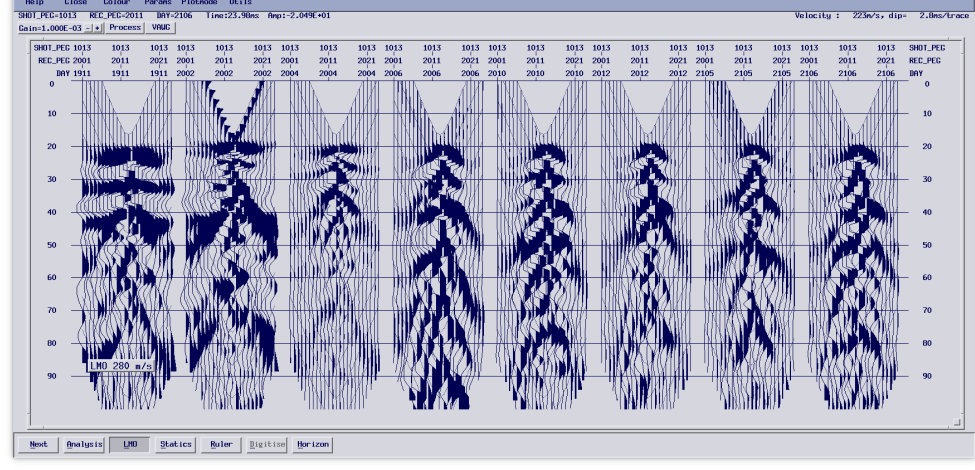


Figure 6. Seismic response of Line 1000 for a source located at SHOT_PEG 1013. (Top) Raw data with the same scaling factor for all campaigns. (Bottom) As in the top panel, but with a linear moveout correction of 280 m/s applied. The header DAY corresponds to the campaign with the following codes: 1911 – November 2019, 2002 – February 2020, 2004 – April 2020, 2006 – June/July 2020, 2020 – October 2020, 2012 – November/December 2020, 2105 – May 2021, 2106 – June 2021.



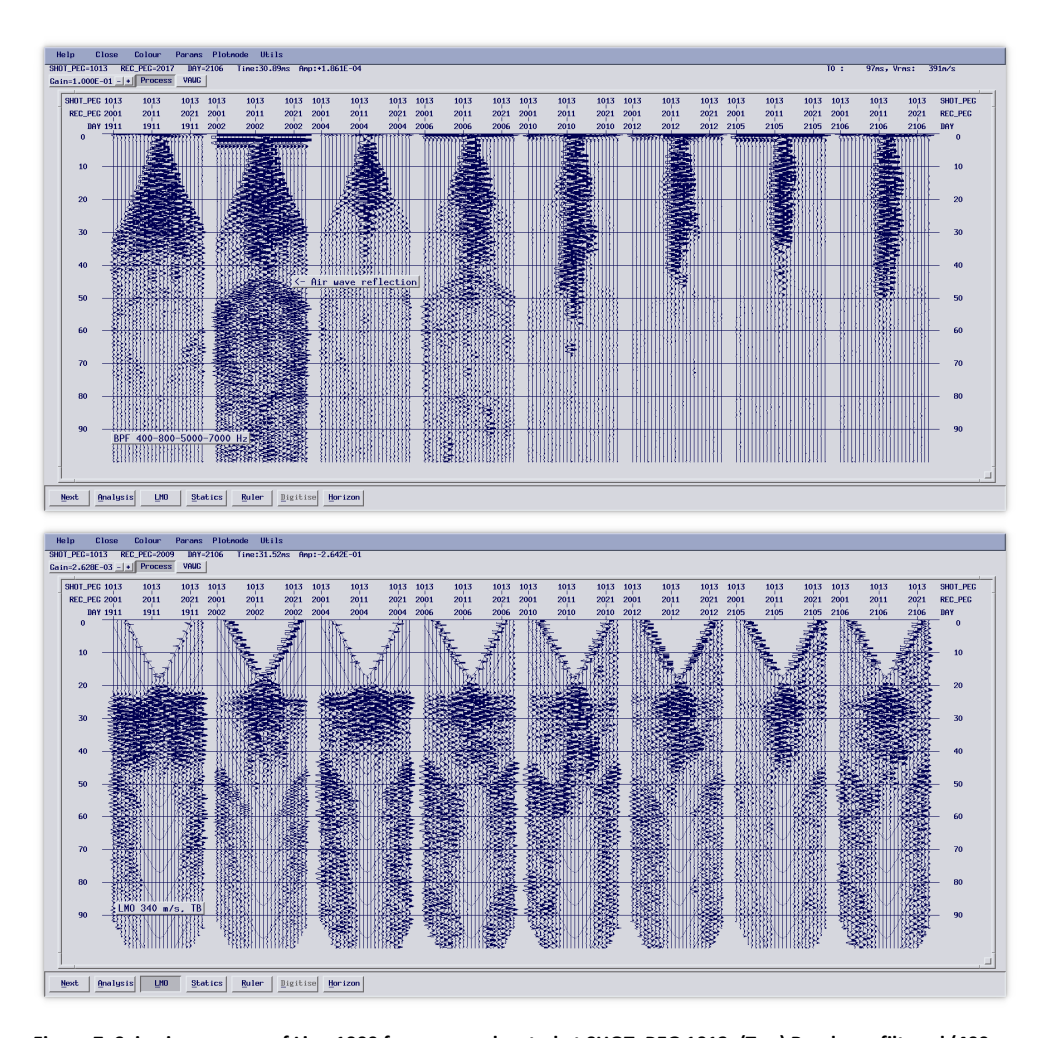


Figure 7. Seismic response of Line 1000 for a source located at SHOT_PEG 1013. (Top) Bandpass filtered (400-800-5000-7000) data with no scaling applied. (Bottom) As in the top panel, but with a linear moveout correction of 340 m/s applied as well as trace balancing. The header DAY corresponds to the campaign with the same codes as in Figure 6.



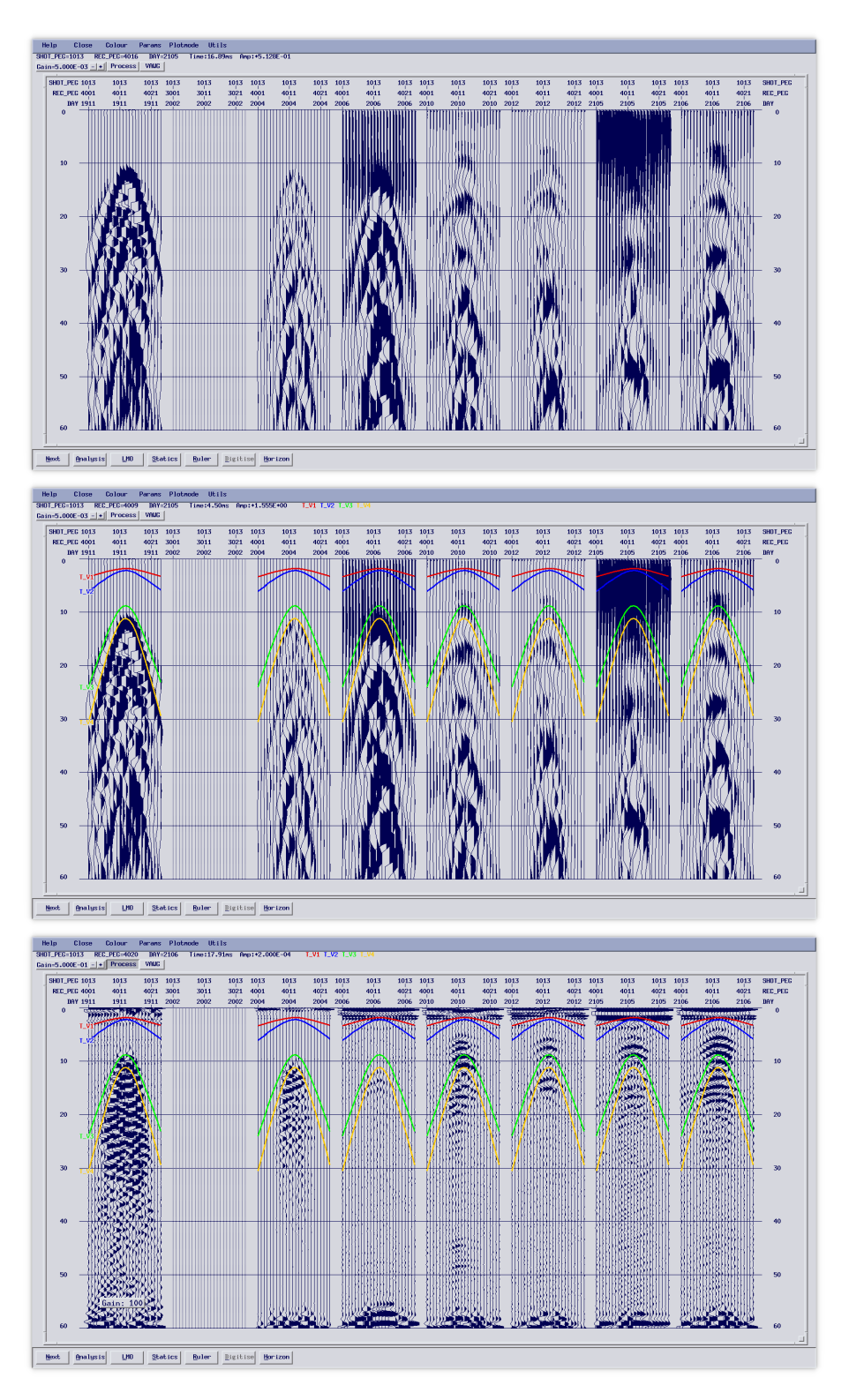


Figure 8. Seismic response of Line 4000 for a source located at SHOT_PEG 1013. (Top) Raw data with no scaling applied. (Middle) As in top, but with arrival times of waves travel with different velocities overlain; red – 4200 m/s plus 1 ms, blue – 1650 m/s, green – 420 m/s, yellow – 340 m/s. (Bottom) As middle panel, but with a bandpass filter of 400-800-5000-7000 Hz applied, as well as a gain of 100 compared to the two upper panels. The header DAY corresponds to the campaign with the same codes as in Figure 6. No data were acquired on the line in the February 2020 campaign.



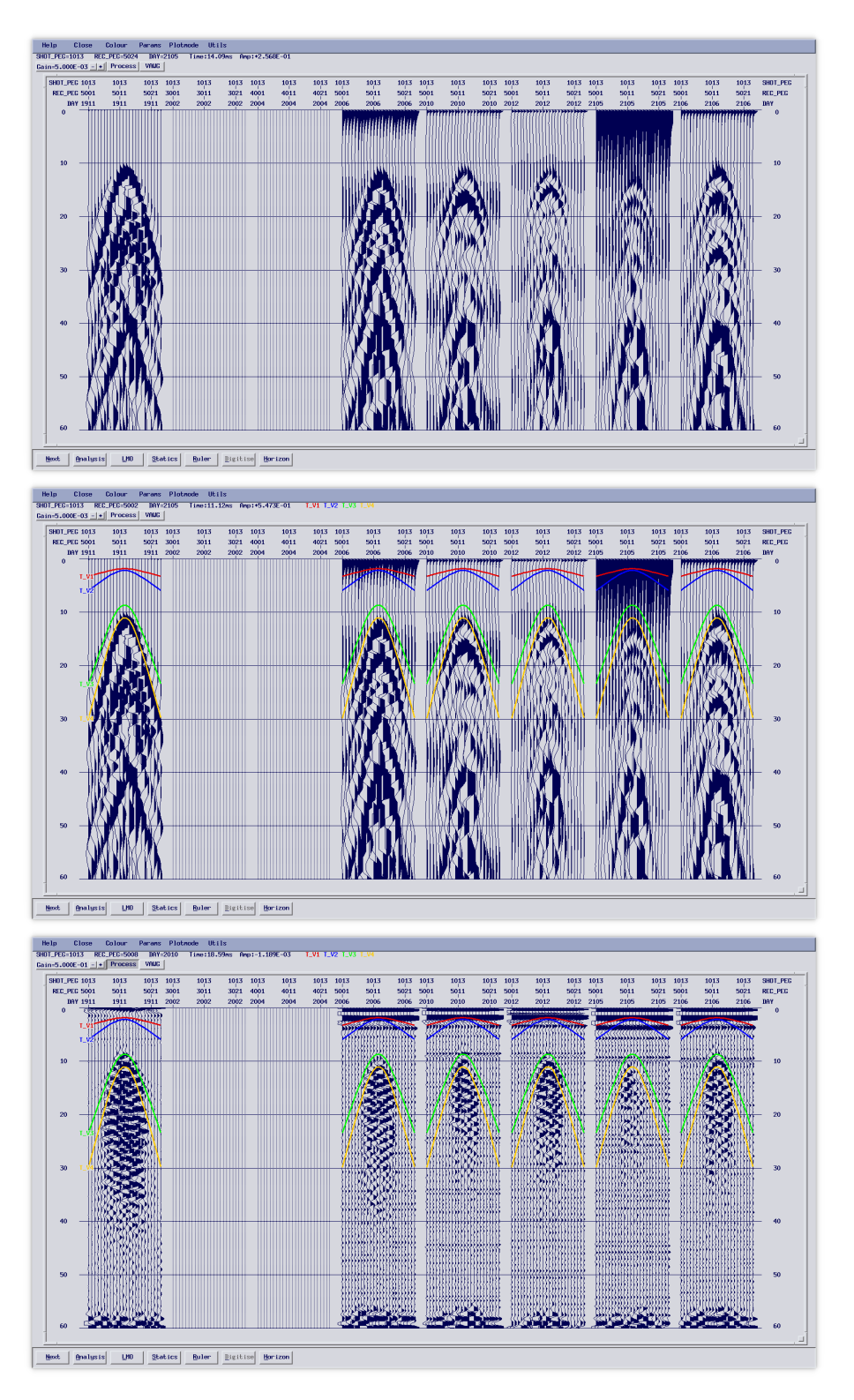


Figure 9. Seismic response of Line 5000 for a source located at SHOT_PEG 1013. (Top) Raw data with no scaling applied. (Middle) As in top, but with arrival times of waves travel with different velocities overlain; red – 4200 m/s plus 1 ms, blue – 1650 m/s, green – 420 m/s, yellow – 340 m/s. (Bottom) As middle panel, but with a bandpass filter of 400-800-5000-7000 Hz applied, as well as a gain of 100 compared to the two upper panels. The header DAY corresponds to the campaign with the same codes as in Figure 6. No data were acquired on the line in the February and April 2020 campaigns.



3.2 SOURCE IN DEEP BOREHOLES

Data acquired with the source in deep borehole 8000 and recorded on line 4000 (bottom upstream) show a distinct pattern with increasing frequency content with time (Figure 10). This is best explained by the dam becoming more and more saturated on the upstream side. No such increase in frequency content is observed on any of the other hydrophone lines. This can be attributed to that these lines are located in the unsaturated zone. Note the distinct increase in frequency content from December 2020 (when the dam was supposedly saturated) to May 2021. Note also that these high frequencies are not observed when shooting in the crest of the dam. This can be explained by the source being within the saturated zone when shooting at deeper levels in borehole 8000, but not on the crest. The first arriving high frequency reflection has a normal moveout velocity of about 1700-1800 m/s and an apex at about 8 ms. This corresponds to a reflector about 7 m away from line 4000. The source to this reflection is discussed later.

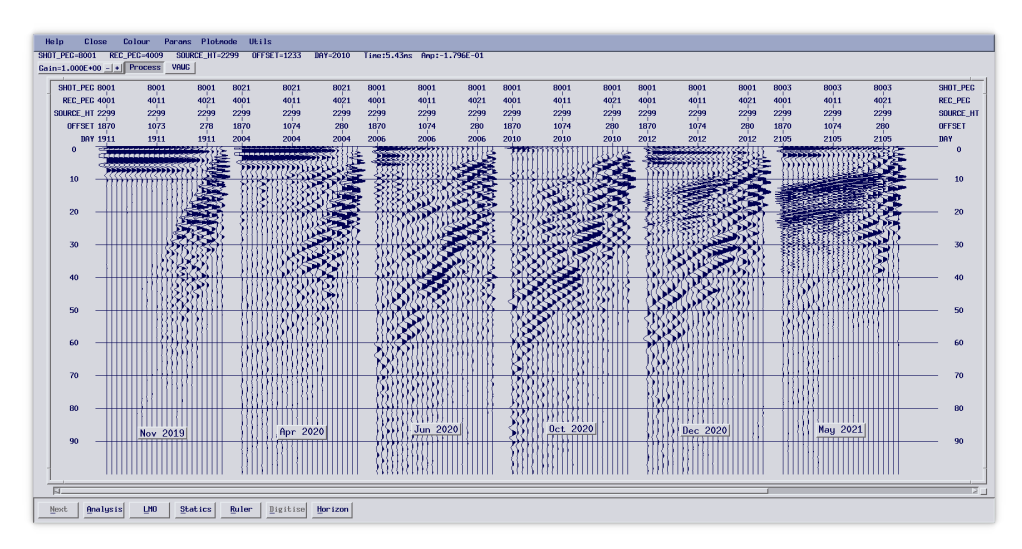


Figure 10. Seismic response of Line 4000 for a source located near the bottom of borehole 8000 (container side upstream). A bandpass filter of 200-400-1500-2000 Hz has been applied, as well as trace balancing. The header DAY corresponds to the campaign with the same codes as in Figure 6. No data were acquired at this source position in February 2020 and June 2021.

3.3 SOURCE IN THE RESERVOIR

In Stage 1 of the project it was noted that much higher frequencies were recorded when shooting in the reservoir compared to shooting in the crest of the dam (Salas-Romero et al., 2021). Figure 11 and Figure 12 show the seismic response at one receiver in the middle of the dam for hydrophone lines 4000 and 5000, respectively. It is clear that high frequencies can be recorded even on line 5000 with this shooting geometry. The red curve in these figures corresponds well to a refracted wave traveling through the concrete base of the dam at 4200 m/s and is the first arrival. The blue curve corresponds to the direct wave propagating through the reservoir, support filling and filters for receiver 4013 and through the reservoir, support filling, filters and core for receiver 5013 with an average velocity of 1650 m/s. The green curve shows the arrival times for a direct wave propagating at an average velocity of 420 m/s. The low frequency nature of this wave suggests that it



may be a shear wave. If this indeed is a shear wave it must have been converted from a P-wave at some point along its travel path since no shear waves can exist in the fluid reservoir. Figure 13 investigates if the arrival times of these waves change with time. The arrivals become more distinct with time, especially the direct arriving P-waves (blue curve). There may even be a slight trend towards earlier arriving P-waves on line 5000, but this is rather unclear. If the P-wave (blue curve) and "S-wave" (green curve) have approximately the same ray path to line 4000 as to line 5000 then an estimate of their velocities through the dam core can be made based on the difference in arrival times on the lines and distance traveled. Calculations give a velocity of about 1550 m/s for the P-wave and 370 m/s for the S-wave. The S-wave estimate assumes that the low frequency arrival in Figure 13 actually represents a shear wave. On lines 2000 and 3000 (not shown here) the arrival of this wave is considerably later, corresponding to a straight ray velocity of c. 200 m/s in the center of the dam. The inconsistent velocities imply that the calculated "S-wave" velocity based on this arrival should be considered unreliable.



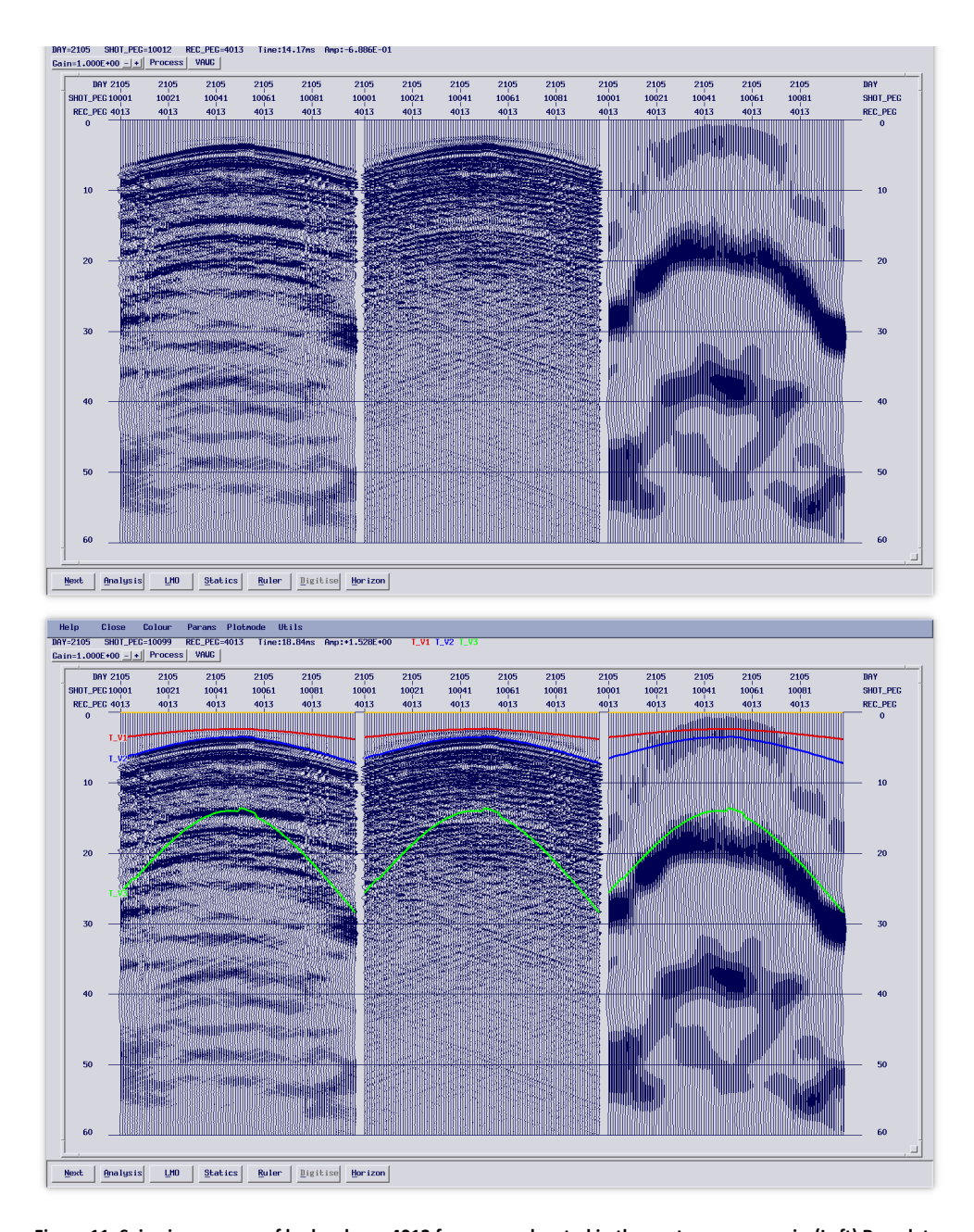


Figure 11. Seismic response of hydrophone 4013 for sources located in the upstream reservoir. (Left) Raw data with trace balancing applied. (Center) Same data after a bandpass filter of 400-800-5000-7000 Hz applied. (Right) Same data as left panel, but with a bandpass filter of 5-10-100-200 Hz applied. Arrival times of waves traveling with different velocities overlain; red – 4200 m/s plus 1 ms, blue – 1650 m/s, green – 420 m/s. The header DAY corresponds to the campaign with the same codes as in Figure 6.



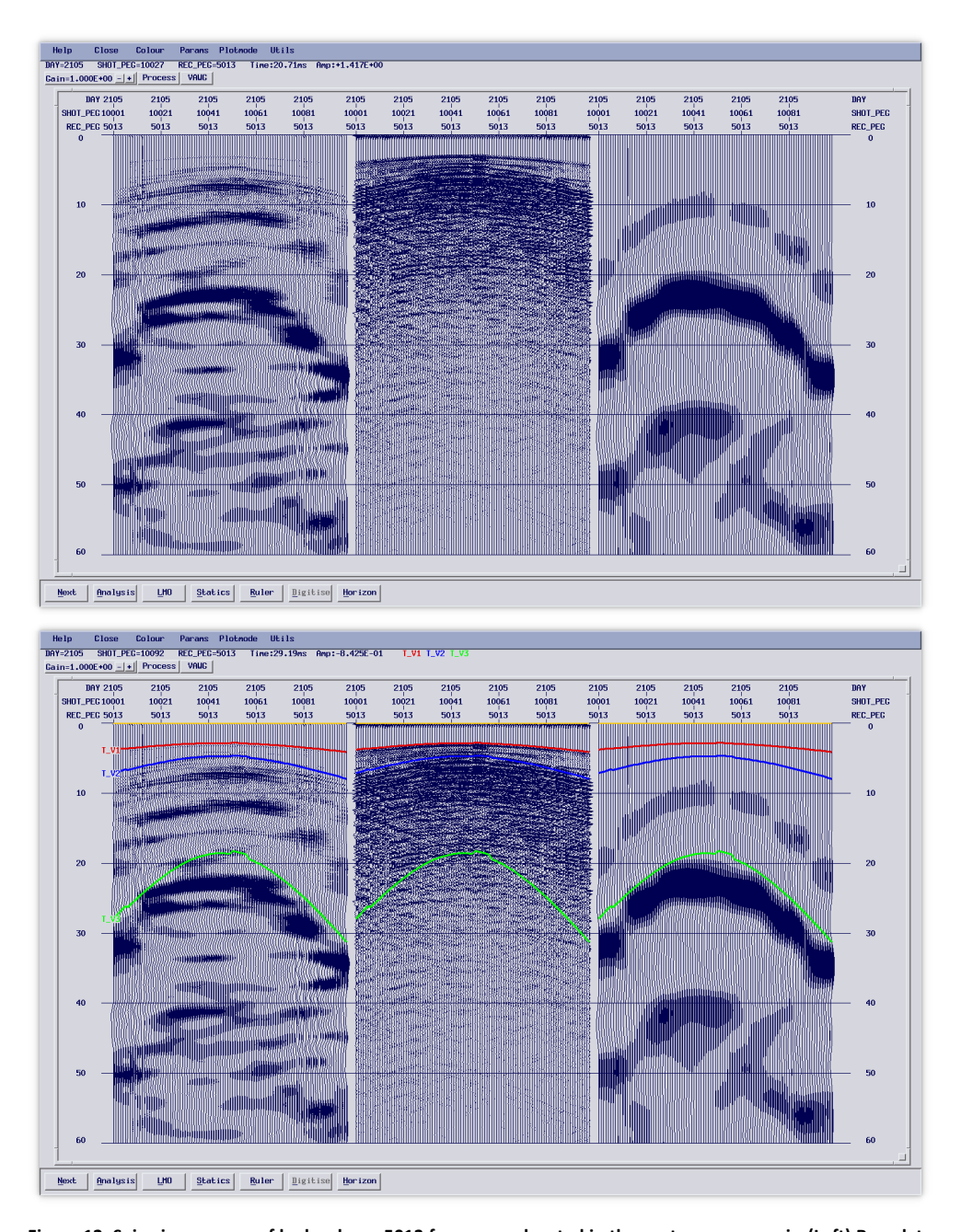


Figure 12. Seismic response of hydrophone 5013 for sources located in the upstream reservoir. (Left) Raw data with trace balancing applied. (Center) Same data after a bandpass filter of 400-800-5000-7000 Hz applied. (Right) Same data as left panel, but with a bandpass filter of 5-10-100-200 Hz applied. Arrival times of waves traveling with different velocities overlain; red – 4200 m/s plus 1 ms, blue – 1650 m/s, green – 420 m/s. The header DAY corresponds to the campaign with the same codes as in Figure 6.



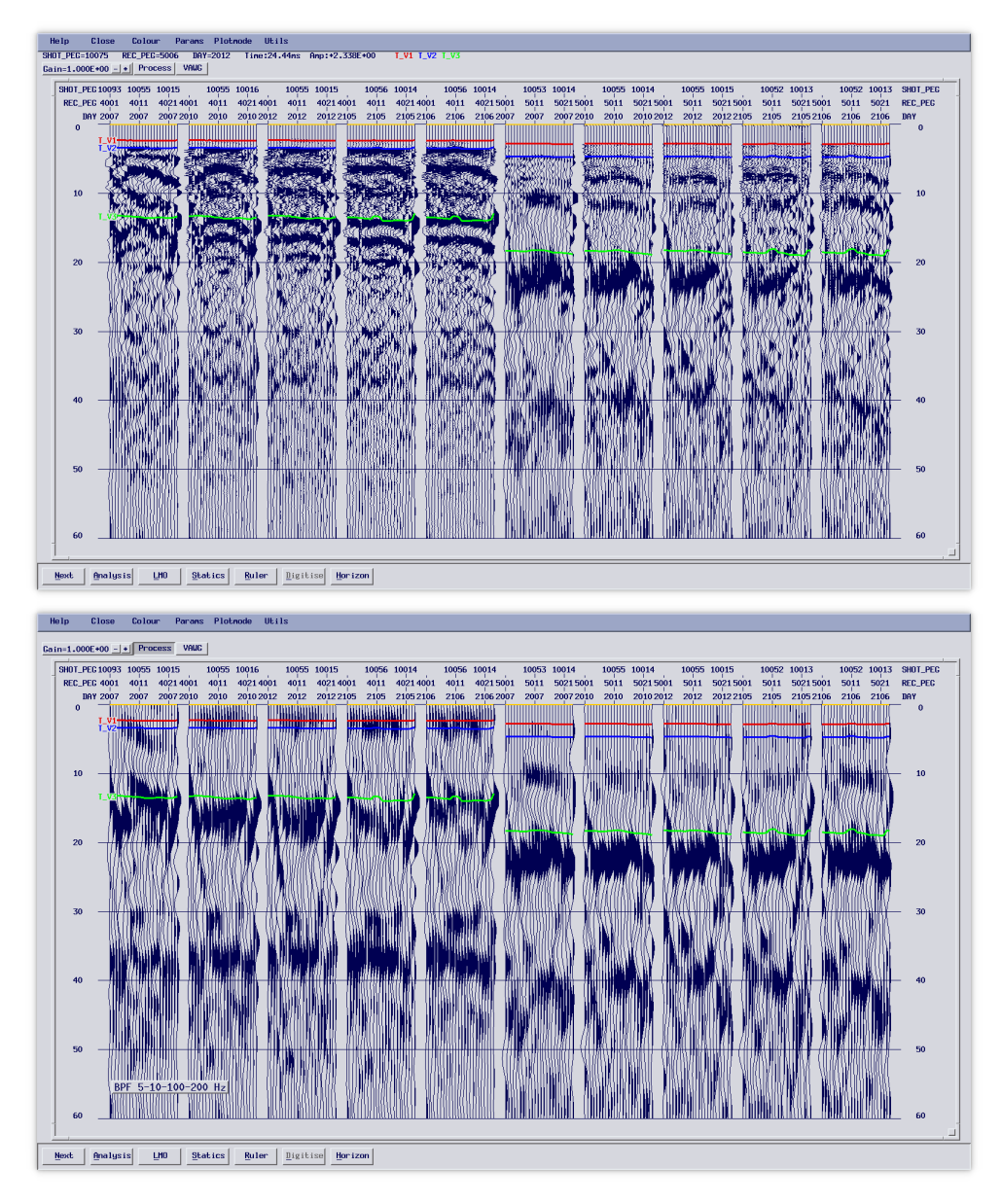


Figure 13. (Top) Seismic response of waves arriving at normal incidence on line 4000 (first 5 panels) and on line 5000 (last 5 panels) with trace balancing applied. (Bottom) Same as top, but with a bandpass filter of 5-10-100-200 Hz applied. Arrival times of waves traveling with different velocities overlain; red – 4200 m/s plus 1 ms, blue – 1650 m/s, green – 420 m/s. The header DAY corresponds to the campaign with the same codes as in Figure 6.

3.4 AMPLITUDE OBSERVATIONS

Shooting in the reservoir should generate fairly consistent source signals, both in phase and amplitude, allowing a comparison of amplitudes of the recorded signals between different campaigns. Figure 14 shows the response from Line 4000 for the source located at approximately the same position in the reservoir for the 5 latest campaigns, from June 2020 to July 2021. Data from each campaign are plotted with the same scaling factor so that amplitudes can be compared directly between campaigns. It is clear that the amplitude response increases with time, an increase in amplitude is even noted between the short period from May 2021 to June 2021.



Note that initially the seismic response is fairly symmetric with decreasing amplitudes of the direct arrival towards the sides of the dam. For the two latest surveys the response is less symmetric with significantly lower amplitudes being recorded at higher receiver numbers (container side of the dam, south side). This suggests that the northern side of the dam was saturating more quickly than the container side. Similar observations can be made for all source locations in the reservoir. Note also that the moveout on the high amplitude arrivals in the first 25 ms corresponds to that of waves having a velocity of about 1650 m/s, implying that the later arrivals are multiples from within the reservoir in this time window. Figure 15 and Figure 16 show the same plots as Figure 14, but for lines 5000 and 2000. Even on these lines the recorded amplitudes clearly increase with time, suggesting that saturation is continuing to increase up until the time of the last survey (June-July 2021).



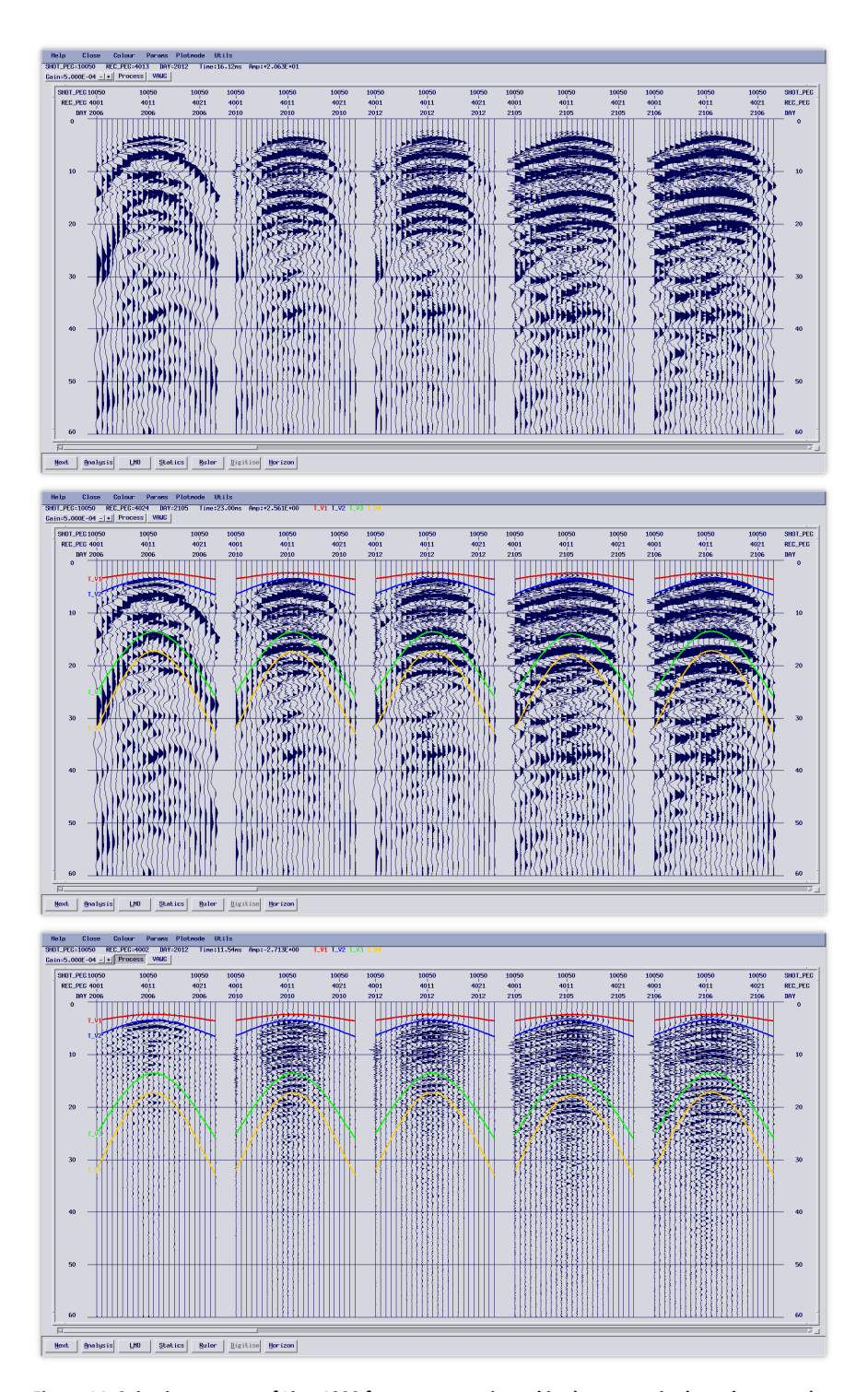


Figure 14. Seismic response of Line 4000 for a source activated in the reservoir along the central part of Cable 1. (Top) Raw data with no scaling applied. (Middle) As in top, but with arrival times of waves travel with different velocities overlain; red – 4200 m/s plus 1 ms, blue – 1650 m/s, green – 420 m/s, yellow – 340 m/s. (Bottom) As middle panel, but with a bandpass filter of 400-800-5000-7000 Hz applied. Gain is the same for all panels and no trace balancing has been applied. The header DAY corresponds to the campaign with the same codes as in Figure 6.



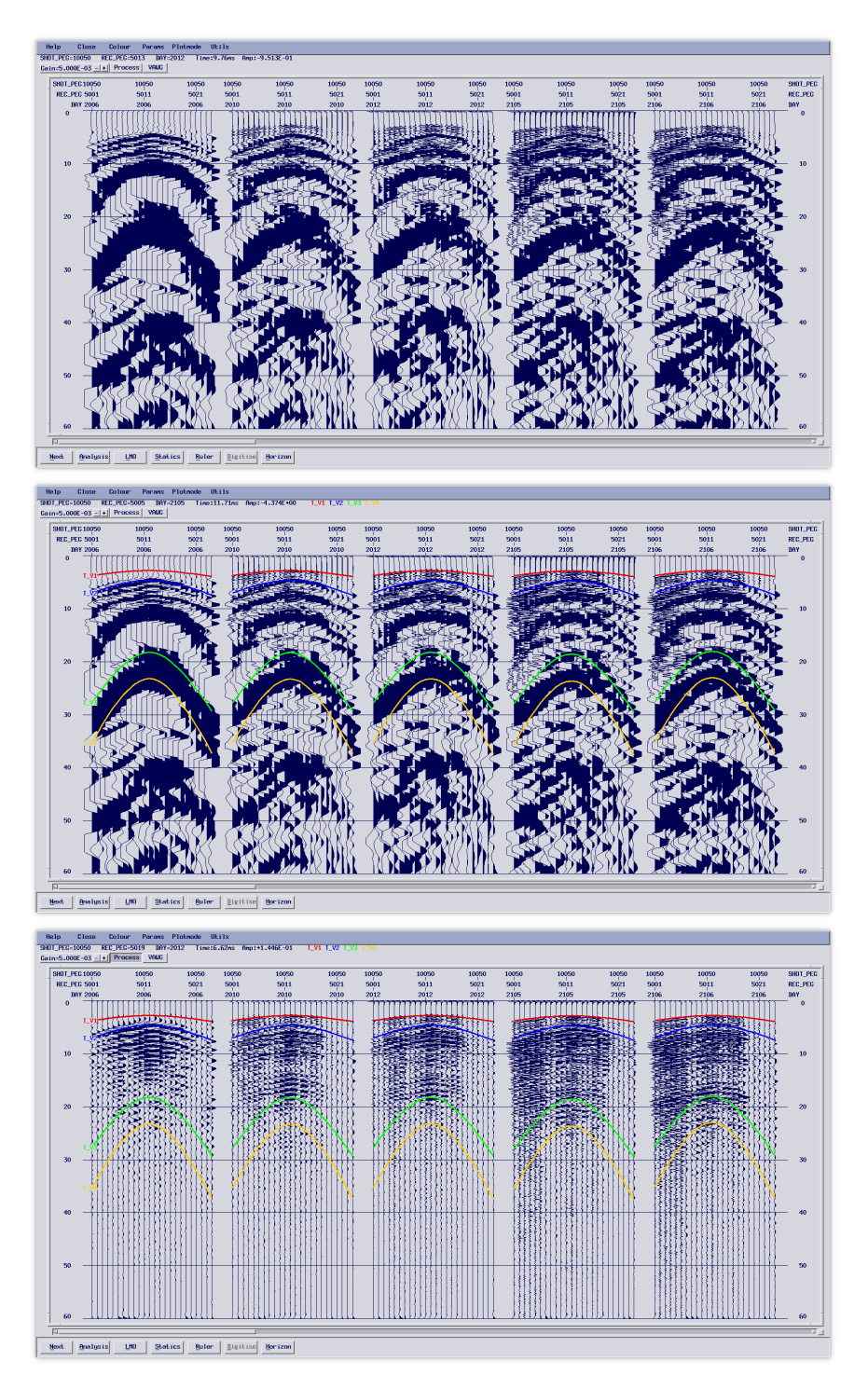


Figure 15. Seismic response of Line 5000 for a source activated in the reservoir along the central part of Cable 1. (Top) Raw data with no scaling applied. (Middle) As in top, but with arrival times of waves travel with different velocities overlain; red – 4200 m/s plus 1 ms, blue – 1650 m/s, green – 420 m/s, yellow – 340 m/s. (Bottom) As middle panel, but with a bandpass filter of 400-800-5000-7000 Hz applied. Gain is the same for all panels and no trace balancing has been applied. The header DAY corresponds to the campaign with the same codes as in Figure 6.



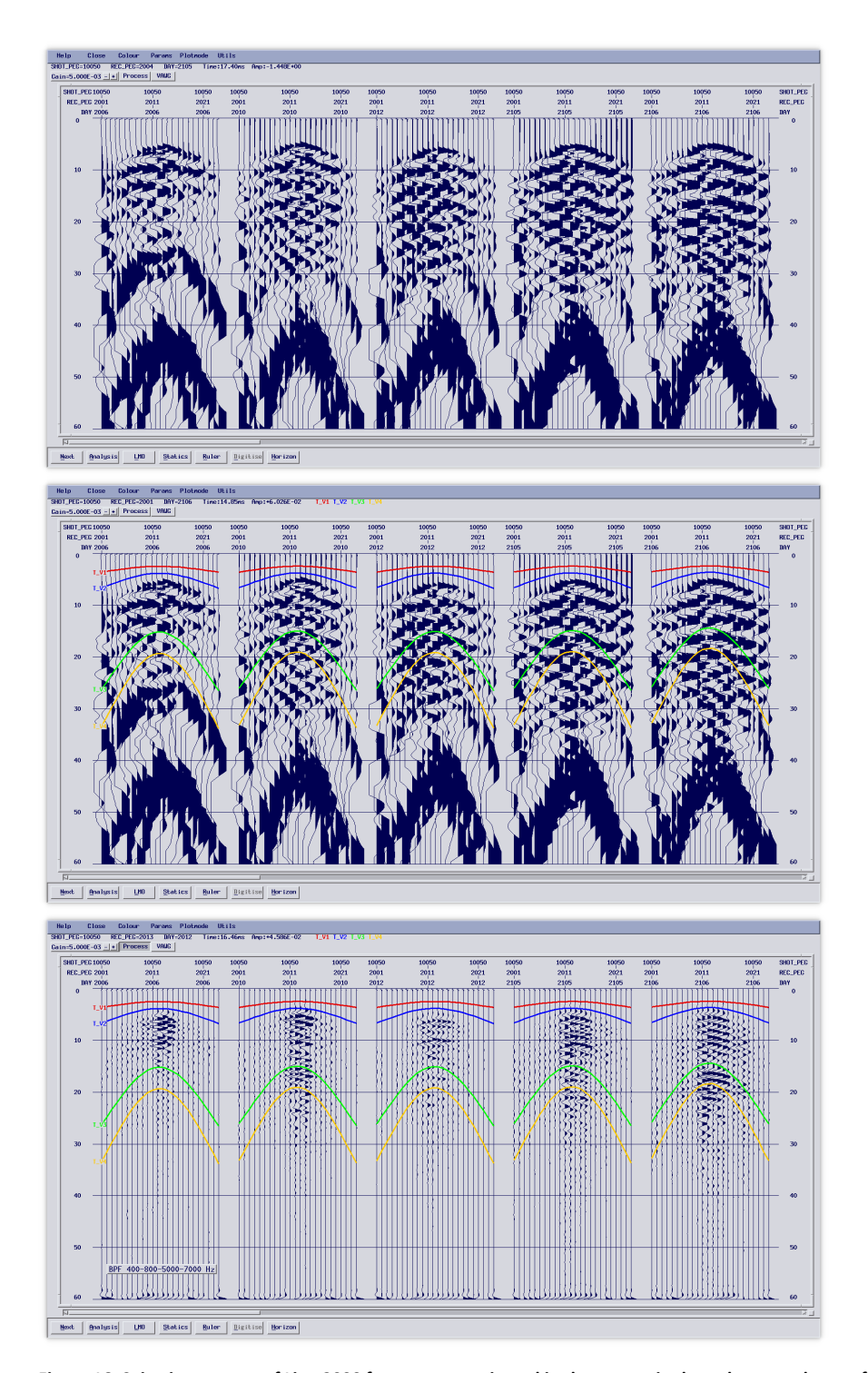


Figure 16. Seismic response of Line 2000 for a source activated in the reservoir along the central part of Cable 1. (Top) Raw data with no scaling applied. (Middle) As in top, but with arrival times of waves travel with different velocities overlain; red – 4200 m – 4200 m/s plus 1 ms, blue – 1650 m/s, green – 420 m/s, yellow – 340 m/s. (Bottom) As middle panel, but with a bandpass filter of 400-800-5000-7000 Hz applied. Gain is the same for all panels and no trace balancing has been applied. The header DAY corresponds to the campaign with the same codes as in Figure 6.



3.5 IDENTIFICATION OF FIRST ARRIVALS FOR VELOCITY DETERMINATION

In order to determine seismic velocities in the dam and monitor changes in properties it is necessary to identify first arrivals for rays with a known path. The geometry of the sources and receivers, as well as the dam structure, makes this a difficult task. Complications are:

- The first arriving wave on lines 4000 and 5000 when shooting in the reservoir is the wave propagating through the concrete block that the dam rests upon. This arrival is very ringy and interferes with later arrivals.
- The direct wave is closely followed by a multiple from the air/water interface (see Figure 17) that arrives about 1 ms after the direct arrival. Later arrivals correspond to waves that are bouncing around in the reservoir (the concrete walls are very good reflectors). These multiples mask later arrivals as well as reflections and/or diffractions.
- It is only when the sensors and sources are in the saturated zone or reservoir that the highest frequencies are recorded.
- The concrete walls on the sides of the crest appear to influence the source when shooting is close to them.

Ideally, shooting and recording in boreholes with the sources in the saturated zone should provide high quality data. The closest to this situation was achieved in the May 2021 campaign when the source was activated at 0.1 m intervals at 31 levels in borehole 8000 and data were recorded on the 3C geophone in borehole 6000 at 1 m depth below the crest (Figure 18). Even under these conditions it is not clear how different arrivals should be interpreted. The seismograms are dominated by a low frequency arrival with a velocity corresponding to 400-500 m/s assuming that the ray path is relatively straight. Most of the energy arrives on the H1 component of the geophone. After highpass filtering at 100-200 Hz and trace balancing an earlier arrival is clearly observed. It has a straight ray velocity corresponding to about 1250 m/s, less than the 1600-1700 m/s expected for the filters. However, its arrival time does correspond to a ray traveling along the concrete wall and diffracting at the upstream corner (Figure 19).

By shooting across the core from BH7000 to BH6000 the signals recorded should represent waves that have mainly traveled through the core and provide direct information on the velocity of it (Figure 20). In order to measure the P-wave velocity accurately, high frequencies are required since the expected traveltime between the borehole is on the order of 1 ms. When filtering at high frequencies significant artifacts are generated at the start of the traces so it is not possible to identify any first arrivals corresponding to the P-wave. However, an arrival with a velocity of c. 1000 m/s is observed at about 4 ms. There is also a clear low frequency arrival at about 20 ms corresponding to a velocity of 100 m/s. These velocities have also been observed on other source-receiver geometries. It is likely that the 100 m/s velocity represents the shear wave velocity of the core.

Figure 21 shows data recorded on line 4000 in May 2021 when shooting at 6 different levels in BH8000. A higher frequency reflection-like event is observed with a normal moveout velocity of about 1700 m/s (the same reflection as seen in Figure 10). It appears to arrive later as the source depth is decreased. The arrival



times at the deeper levels correspond well with a wave that travels down the concrete side and then diffracts, but also to a reflection off the upstream concrete wall. In fact, the shape of the curve fits better when assuming the reflection is off the upstream concrete wall. Note also the refraction along the concrete base and the direct wave through the filter are clearly seen in the seismograms when the source is at deeper levels.

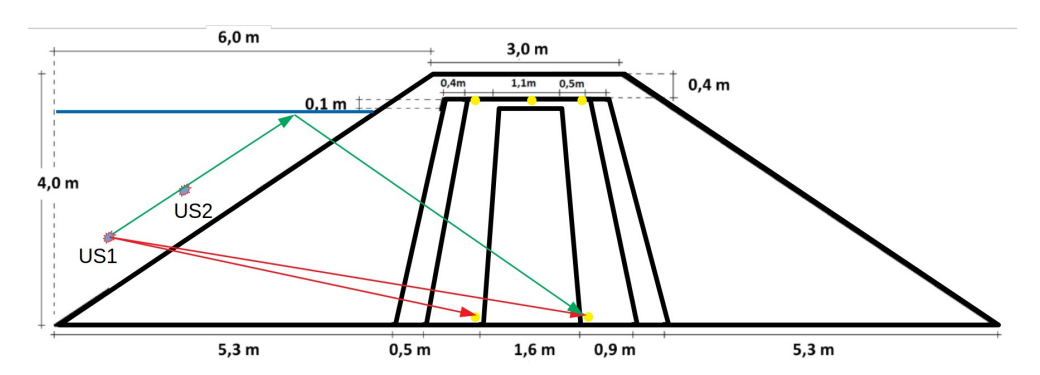


Figure 17. Cross section of dam geometry and location of hydrophone sensors and source locations in the reservoir.



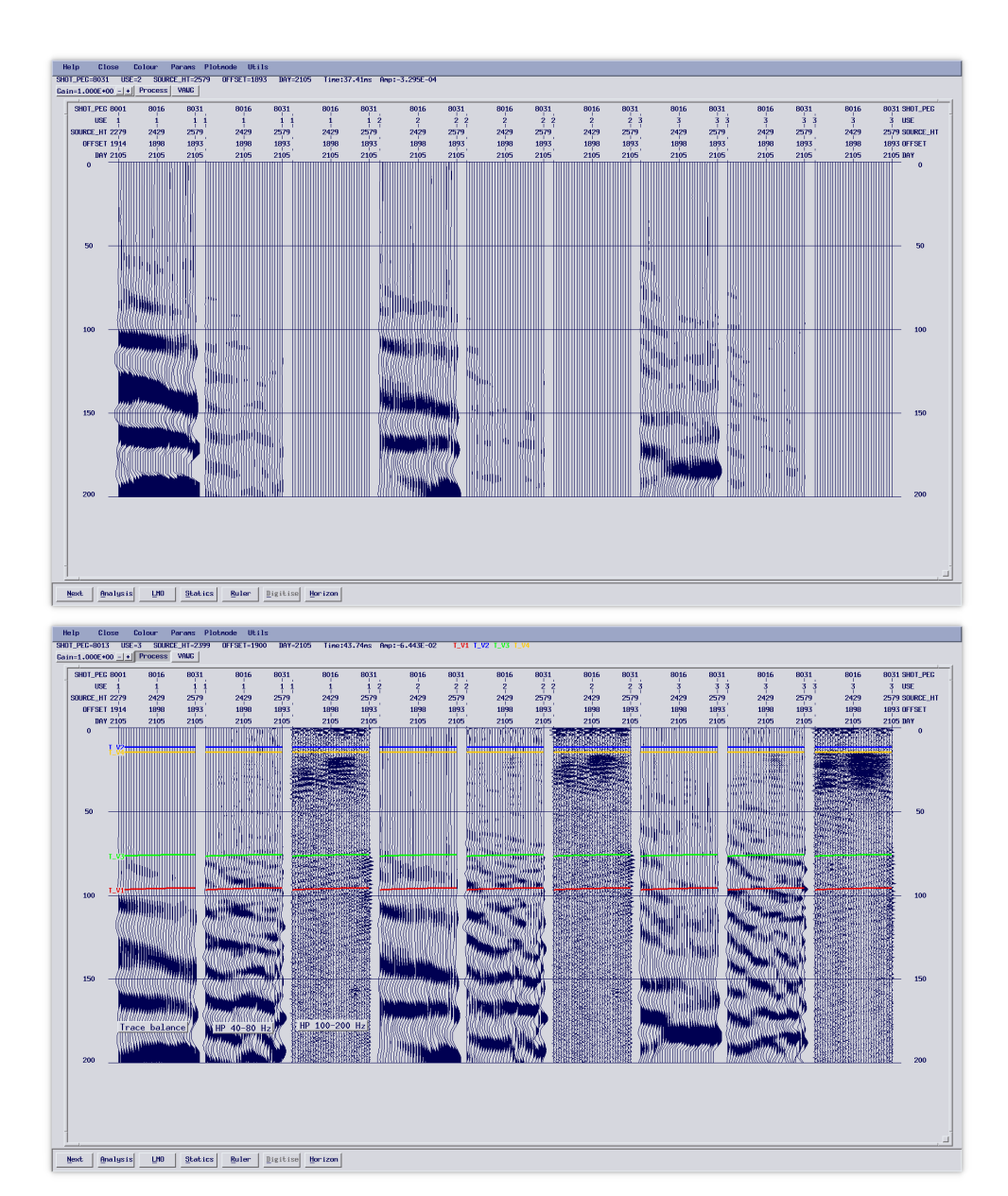


Figure 18. (Top) H1, H2 and V components of the 3C geophone recording data in BH6000 at 1 m depth for source in BH8000 activated at 0.1 m intervals. First three panels are H1 consisting of raw data, highpass filtered at 50-80 Hz and highpass filtered at 100-200 Hz. Second three panels are the same, but for the H2 component, last three panels are the same, but for the V component. No trace balancing has been applied. (Bottom) Same as top plot, but with trace balancing applied and with arrival times of waves traveling with different velocities overlain; red – 400 m/s, blue – 1650 m/s, green – 500 m/s, yellow – diffraction from concrete corner in the reservoir arriving at 1900 m/s. The header DAY corresponds to the campaign with the same codes as in Figure 6.



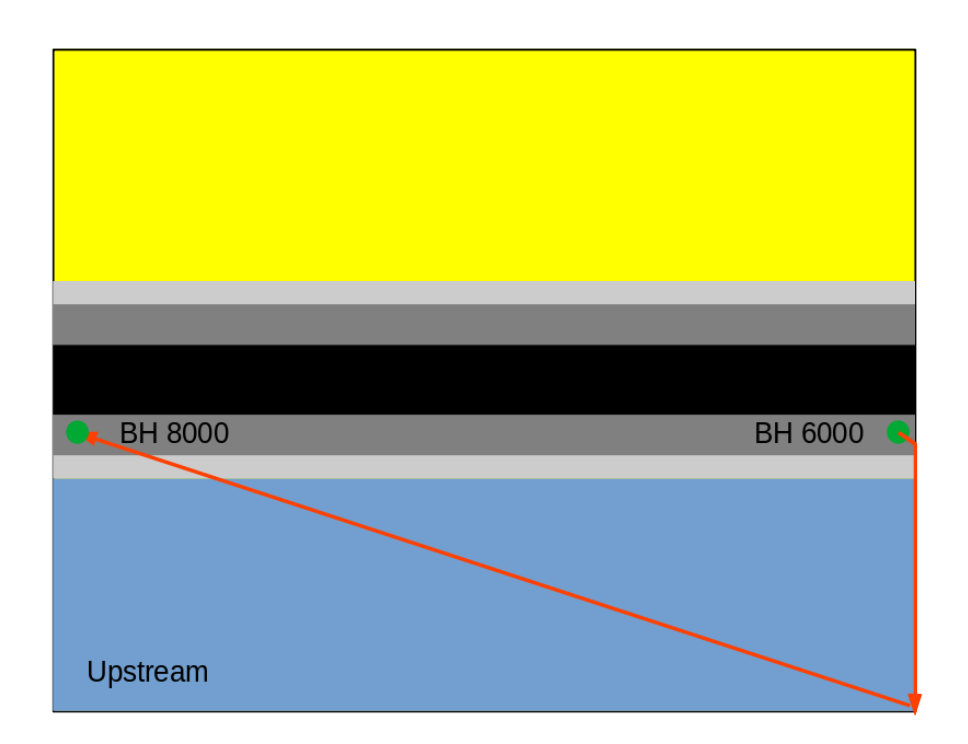
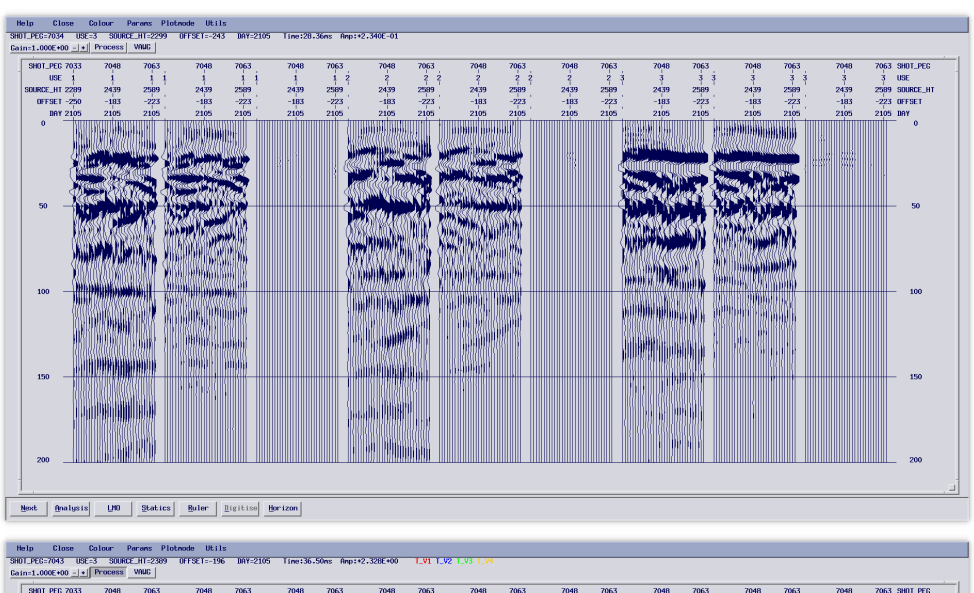


Figure 19. Plan view of dam geometry and location of hydrophone sensors and source locations in the reservoir. Ray paths shown may explain the high frequency arrival in Figures 14 and 16.





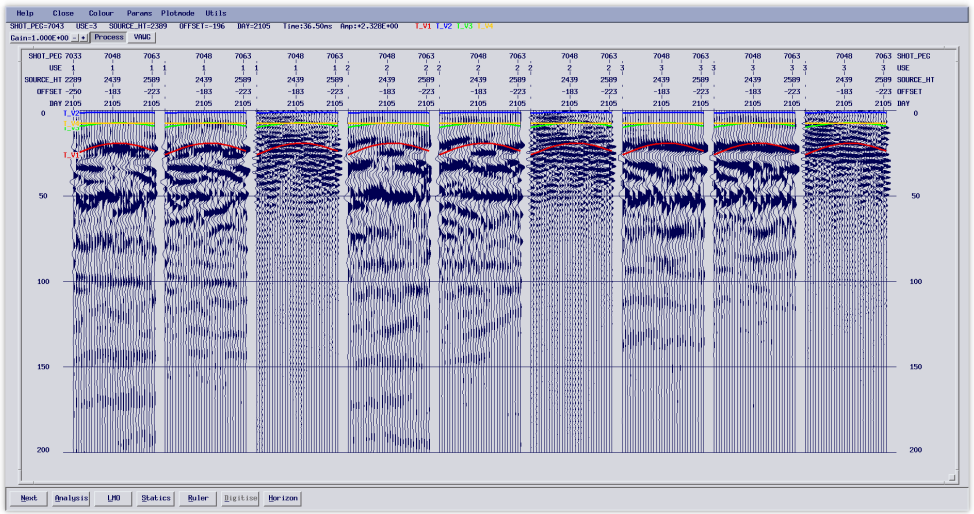


Figure 20. (Top) H1, H2 and V components of the 3C geophone recording data in BH6000 at 2 m depth for source in BH7000 activated at 0.1 m intervals. First three panels are H1, consisting of raw data, highpass filtered at 50-80 Hz and highpass filtered at 100-200 Hz. Second three panels are the same, but for the H2 component, last three panels are the same, but for the V component. No trace balancing has been applied. (Bottom) Same as top plot, but with trace balancing applied and with arrival times of waves traveling with different velocities overlain; red – 100 m/s, blue – 1650 m/s, green – 500 m/s, yellow – diffraction from concrete corner in the reservoir arriving at 1900 m/s. The header DAY corresponds to the campaign with the same codes as in Figure 6.



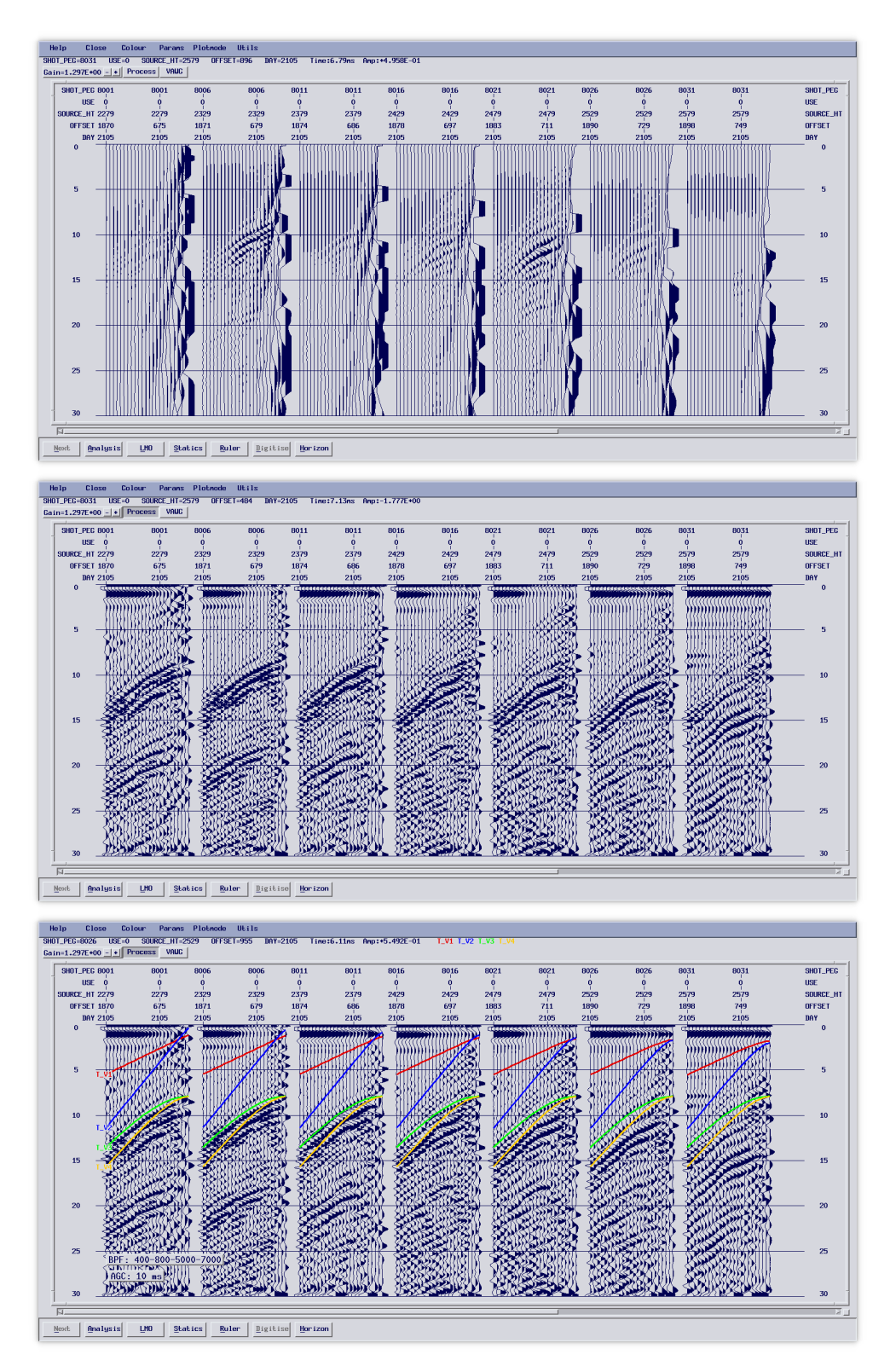


Figure 21. Line 4000 seismic response for source in BH8000 activated at 0.5 m intervals. (Top) Raw data with no trace balancing applied. (Middle) Bandpass filter 400-800-5000-7000 Hz and AGC of 10 ms applied. (Bottom) As middle, but arrival times of different wave s overlain; red – 4200 m/s, blue – 1650 m/s, green – reflection off upstream concrete wall arriving with a velocity of 1700 m/s, yellow – diffraction from concrete corner in the reservoir arriving at 1700 m/s. The header DAY corresponds to the campaign with the same codes as in Figure 6.



3.6 ESTIMATES OF V_P AND V_S VELOCITIES AND POSSIBLE CHANGES WITH TIME

In Stage 1 of the project Vp and Vs were estimated to be on the order of 450-1100 m/s and 110-140 m/s in the core, respectively (Salas-Romero et al., 2021). The higher values corresponding to deeper in the dam. These values are consistent with observations in this study. Table 1 gives our current best estimates of the velocities in the dam. In Stage 1, velocities within the bottom part of the core were interpreted to increase with time up until December 2020. In the data analyzed here there are signs of an increasing velocity trend from July 2020 to July 2021 through the bottom part of the core (Figure 13), but this is only a weak trend and cannot be quantified. The geometrical setup of the sources and receivers was not optimal for determining the velocities of the dam and monitoring changes.

Table 1. Current best estimates of velocities in the dam. Note that the core may not be fully saturated from a seismic viewpoint.

Scisine viewpoint.					
Vp "saturated"	Vp dry	Vs			
1550	400	120			
1700	250	120			
Not relevant	4200	No estimate			
	"saturated" 1550 1700	"saturated" 1550 400 1700 250			



4 Data evaluation

4.1 POTENTIAL DEFECTS

In Stage 1 of the project (Salas-Romero et al., 2021) five locations with potential defects were identified. This was based on analyses of data from the first 6 campaigns. However, there was a general lack of consistency in the seismic response from one campaign to the next and no clear diffractions were observed in two consecutive campaigns from the same location. Two additional surveys were performed during the current phase. Since the data analyses presented in this report show that it is probably only data recorded on hydrophone line 4000 with the source in the reservoir that have high enough frequencies to detect any diffractions the focus has been on analyses on this configuration. Figure 22 shows stacked sections from campaigns 5-8, corresponding to data acquired in October 2020, November 2020, May 2021 and June 2021. An increased amplitude is noted at about 5 m along the profile with signs of a diffraction pattern on all four sections. However, none of the defects were centered at 5 m along the dam (measured from the south side). The closest one was a concrete cube at 4 m (Lagerlund et al, 2022). Unless the anomaly is an interference effect due to two or more of the defects we also conclude in this phase that it was not possible to detect any of the defects with the methodology used.

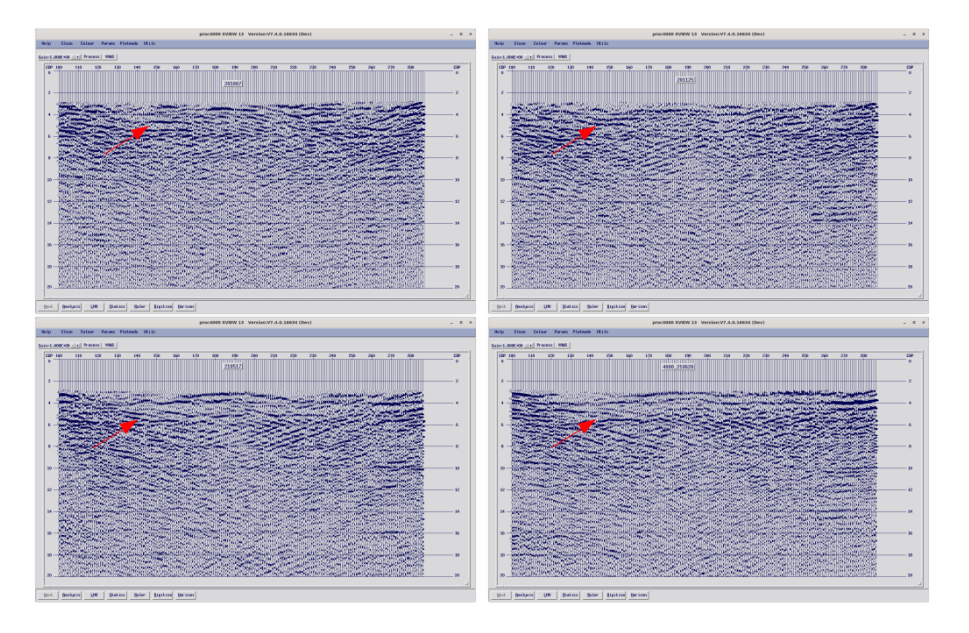


Figure 22. Stacked sections with source in the reservoir and recording on line 4000. Data are from campaigns October 2020, November 2020, May 2021 and June 2021. Red arrows point to a potential anomaly representing a defect about 5 m north of the south side of the dam.

4.2 SEISMIC MODELING

In order to investigate more comprehensively the expected seismic response from the defects and determine if any of them should be apparent on the seismic data 3D seismic modeling was performed for all of six defects (Table 2) using the



current best estimates of the P-wave velocities of the dam. Figure 23 shows the velocity model for Defect 1. The boundary between the saturated core with high velocity and the unsaturated core with low velocity is modeled, rather simplistically, as a planar boundary. This is rather unrealistic and produces unwanted reflections, perhaps masking the signal from the defects. For the modeling, line 4000 was used for the receivers and the sources were in the reservoir with a geometry similar to that shown in Figure 17. An acoustic finite difference code from the open source software package Madagascar (www.ahay.org) was used to perform the modeling. The source function used had an amplitude spectrum in the 2000-4000 Hz range. After generation of the source gathers, the synthetic data were sorted and stacked in a manner similar to that as applied to the observed data.

Modeling results from the six defects are shown in Figure 24. For five of the six defects it is very difficult to see any signs of the defects in the stacked sections. Interference from reflections generated at boundaries within the model and from the sides mask the diffractions. Only Defect 3 has a visible response. This is likely due to its elongated shape relative to the seismic wavefield, resulting in constructive interference.

In many geophysical applications it is difficult to identify anomalies by simply looking at a single snapshot in time, for example in monitoring injected CO2 in the subsurface. However, if a baseline image is subtracted from the image containing the anomaly then the presence of the anomaly is easier to identify. Figure 25 shows the difference between the images shown in Figure 24 and a baseline image that was generated from a model with no defects. Now the diffracted nature of the defect response is apparent on all sections. Note the response from Defect 3 has the highest amplitude, as expected. This suggests that even if it was not possible to detect the defects at the Älvkarleby experimental dam it may be possible to detect changes within a dam if surveys can be repeated under similar conditions. This would allow the development of new defects to be monitored.

Note that the actual response of the dam to the defects is the summation of the difference responses in Figure 25 for the six defects (Figure 26). Since the responses from the defects interfere with one another this further complicates the problem of detecting a single defect.

Table 2. List of defects that were built into the dam (Lagerlund et al., 2022).

, ,							
No.	Type	Shape	Size (m)	х	y	Z	
1	Cavity	Cube	$0.4 \times 0.4 \times 0.4$	13.0	7.5	1.0	
2	Permeable zone	Square	0.5×0.1	10.0	7.5	2.5	
3	Vertical loose zone	Circular	0.3 x 2.5	7.0	7.5	2.3	
4	Boulder	Cube	$0.5 \times 0.5 \times 0.5$	4.0	7.5	2.0	
5	Permeable zone	Square	0.2×0.2	0.0	7.5	3.0	
6	Fine filter defect upstream	Square	0.3 x 0.3 x 0.5	15.0	6.6	1.3	



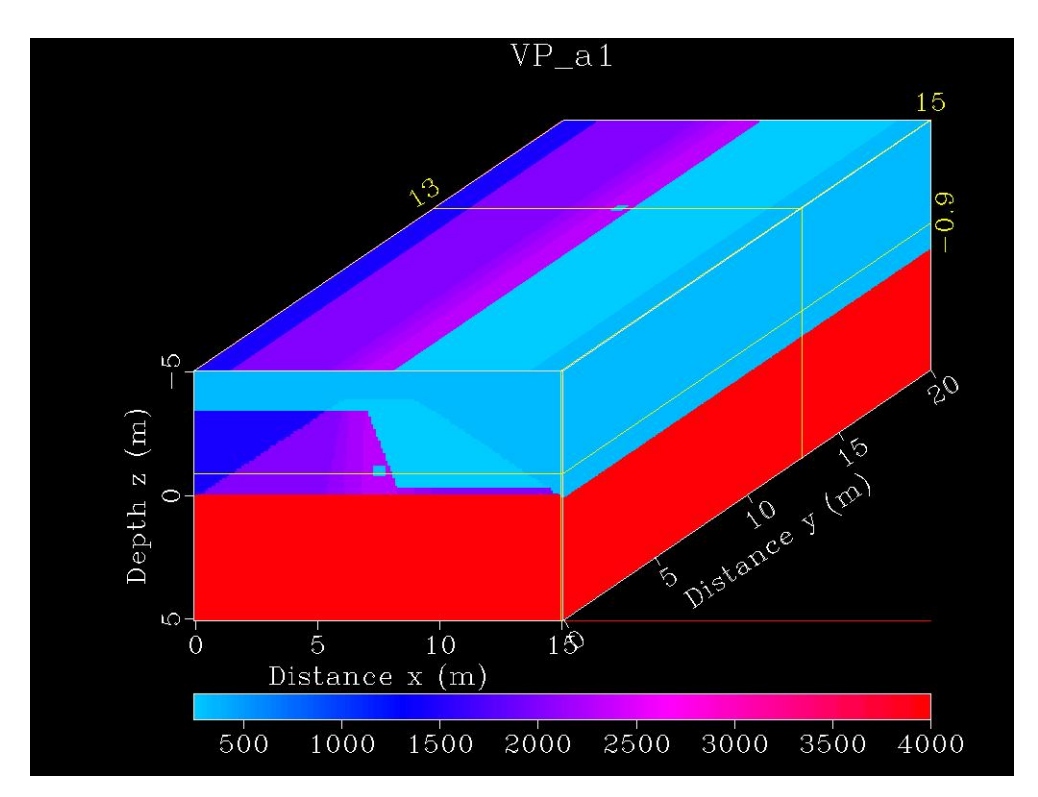


Figure 23. Velocity (P-wave) model for Defect 1. The yellow lines indicate where the cuts in the model are for the surfaces shown on the front (x-z plane) and top (x-y plane) are displayed.



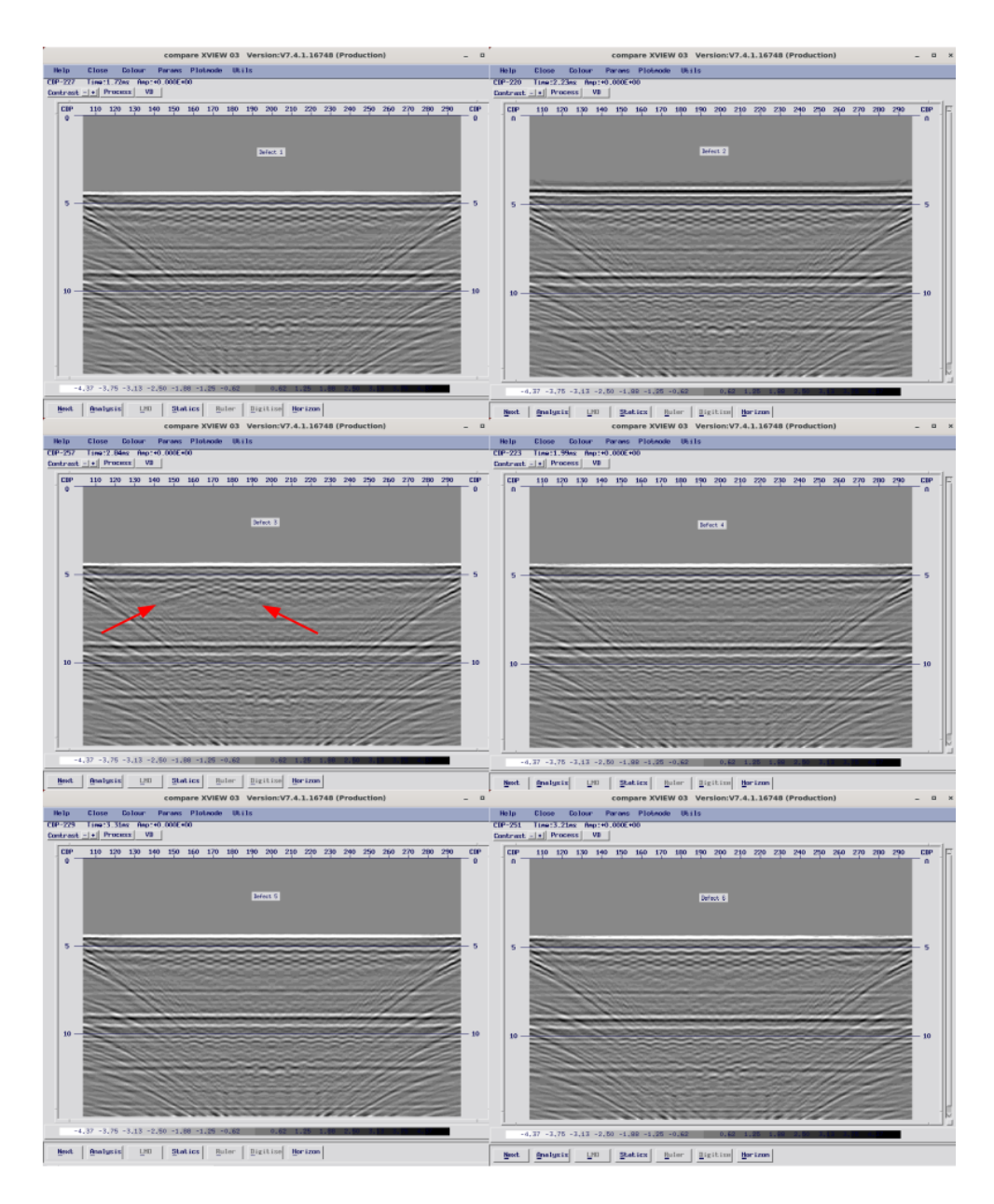


Figure 24. Stacked section for the six defects. Only Defect 3 (middle-left) has a clear diffraction response (red arrows). Same scaling has been applied to all sections.



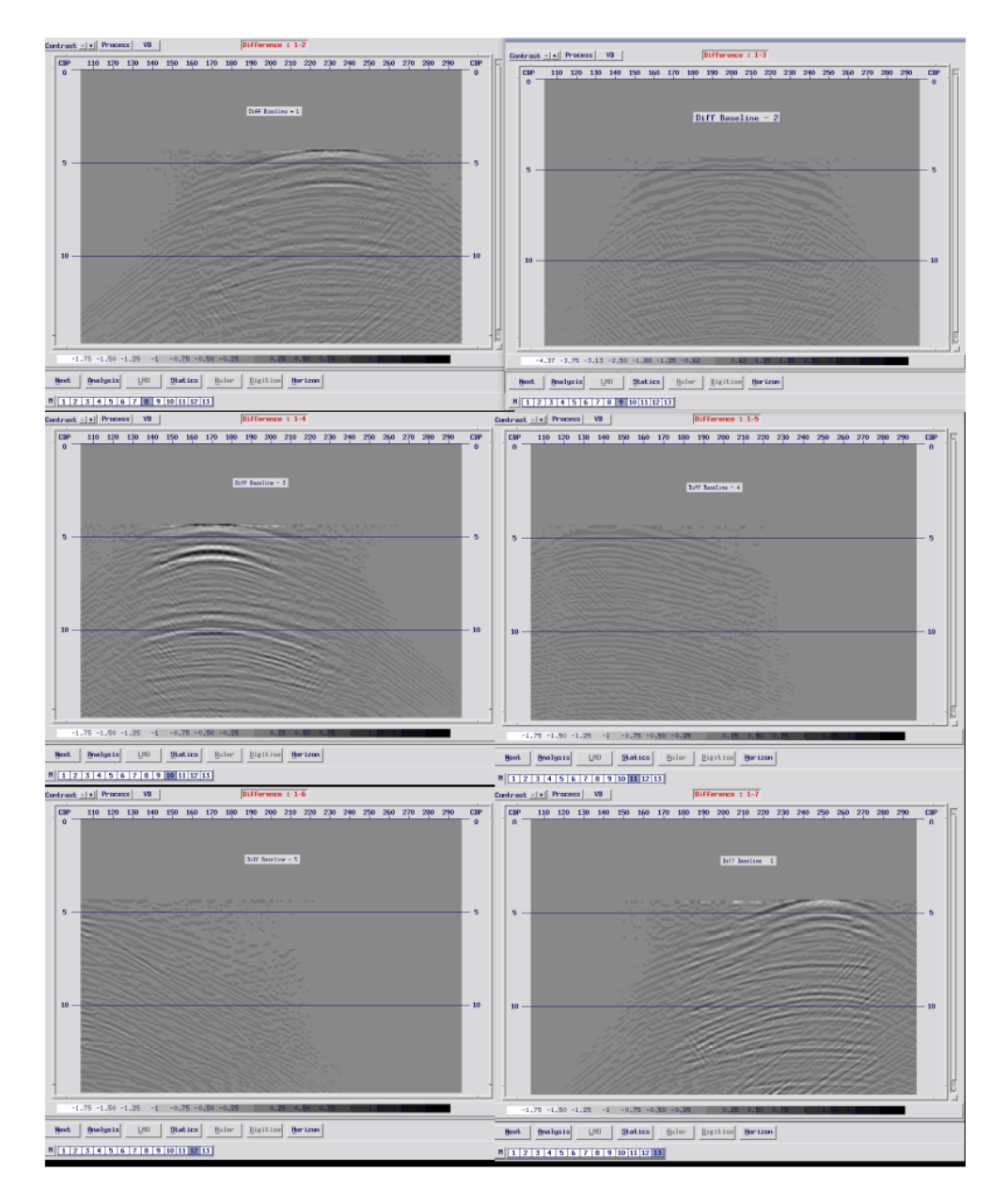


Figure 25. Difference sections for the six defects. A baseline survey with no defects has been subtracted from each of the six sections in Figure 4.2.2. Same scaling has been applied to all sections.



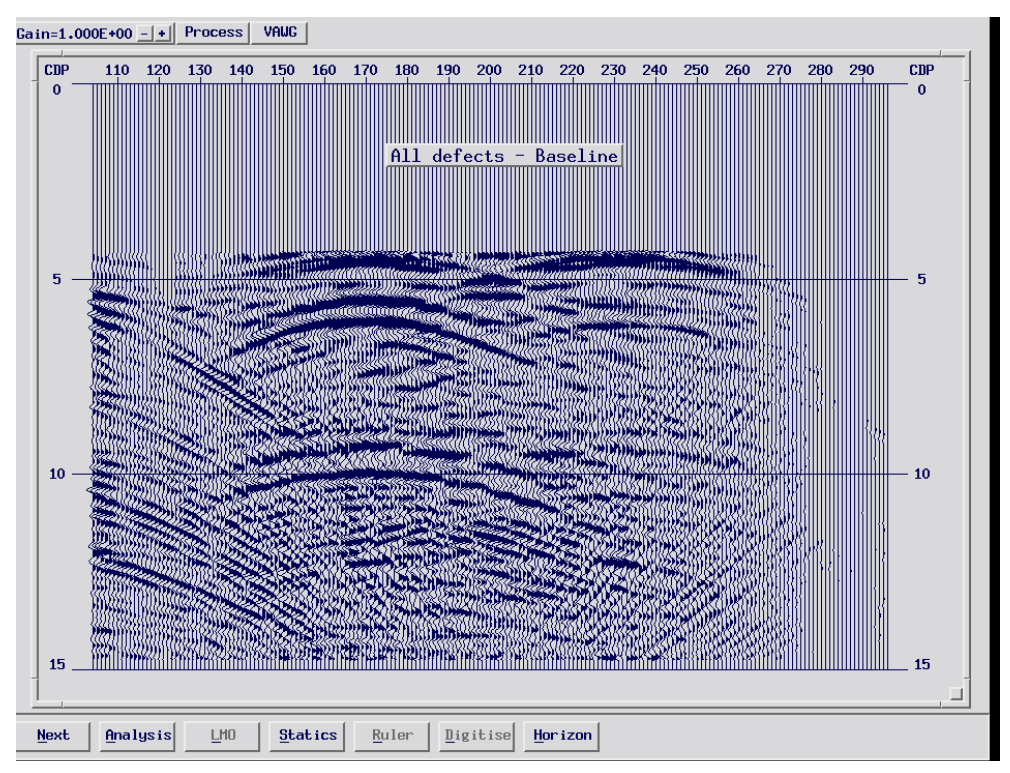


Figure 26. Seismic response of all defects combined. This is a simulation of the total expected signature of the defects and represents the result when a baseline is subtracted.

4.3 OUTLOOK

Salas-Romero et al. (2021) summarized the lessons learned from Stage 1. These lessons are still valid and will not be reproduced here except some more detail concerning the geometry of the sources and receivers. We also suggest some future studies that could be performed on an existing real dam.

From the analyses in Stage 1 and this study it is clear that all sources and receivers should be in the saturated zone in order to record the required high frequencies for imaging, but even for picking P- and S-wave arrivals for velocity determination. Figure 27 shows an example of a geometry that would have been better to have been employed. In this case all five hydrophone lines are on the upstream side of the core and located in the fine filter below the top of the reservoir water level. In addition to providing higher quality data in this configuration, it would also have permitted defects to be imaged better at different levels in the core (Figure 28). In order to measure velocities more accurately, and as a function of time, two boreholes with permanently installed geophones could have been instrumented on both sides of the core. If 8 levels in each borehole with three components recorded per level were to be used this would then require an additional 48 channels. This is in addition to the 120 channels used for the hydrophone recordings. However, the capability to clearly distinguish P-waves from S-waves and directly compare seismograms from fixed locations would be a great advantage. Furthermore, rather than having a cable for hanging the sparker source from it would be better to have a fixed rail that the source could slide along. This would significantly improve the



repeatability of the source locations, allowing a better comparison between campaigns, and also a more consistent signal within campaigns.

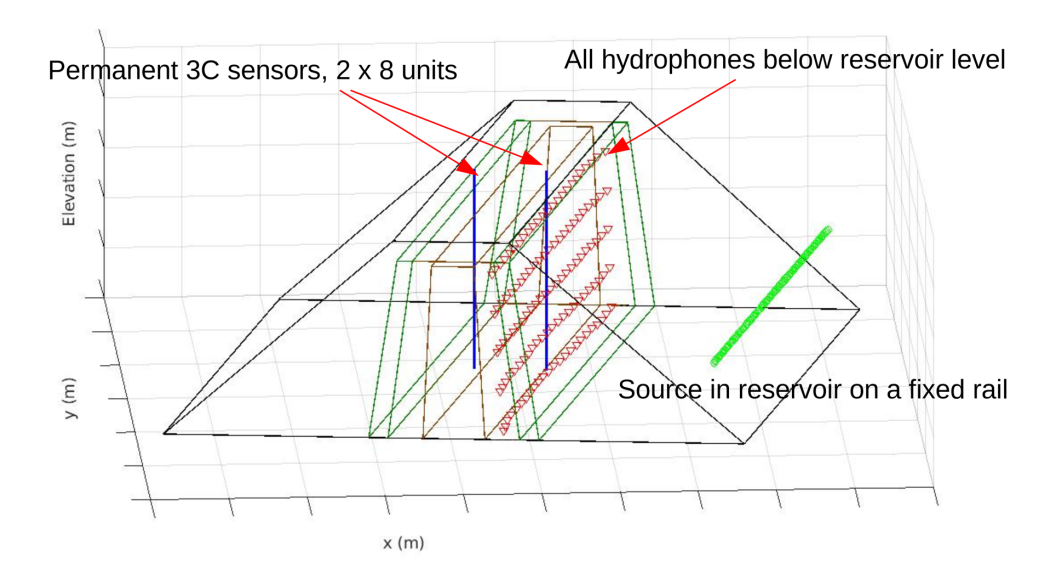


Figure 27. Suggested geometry of sources and receivers if the experiment were to be repeated.



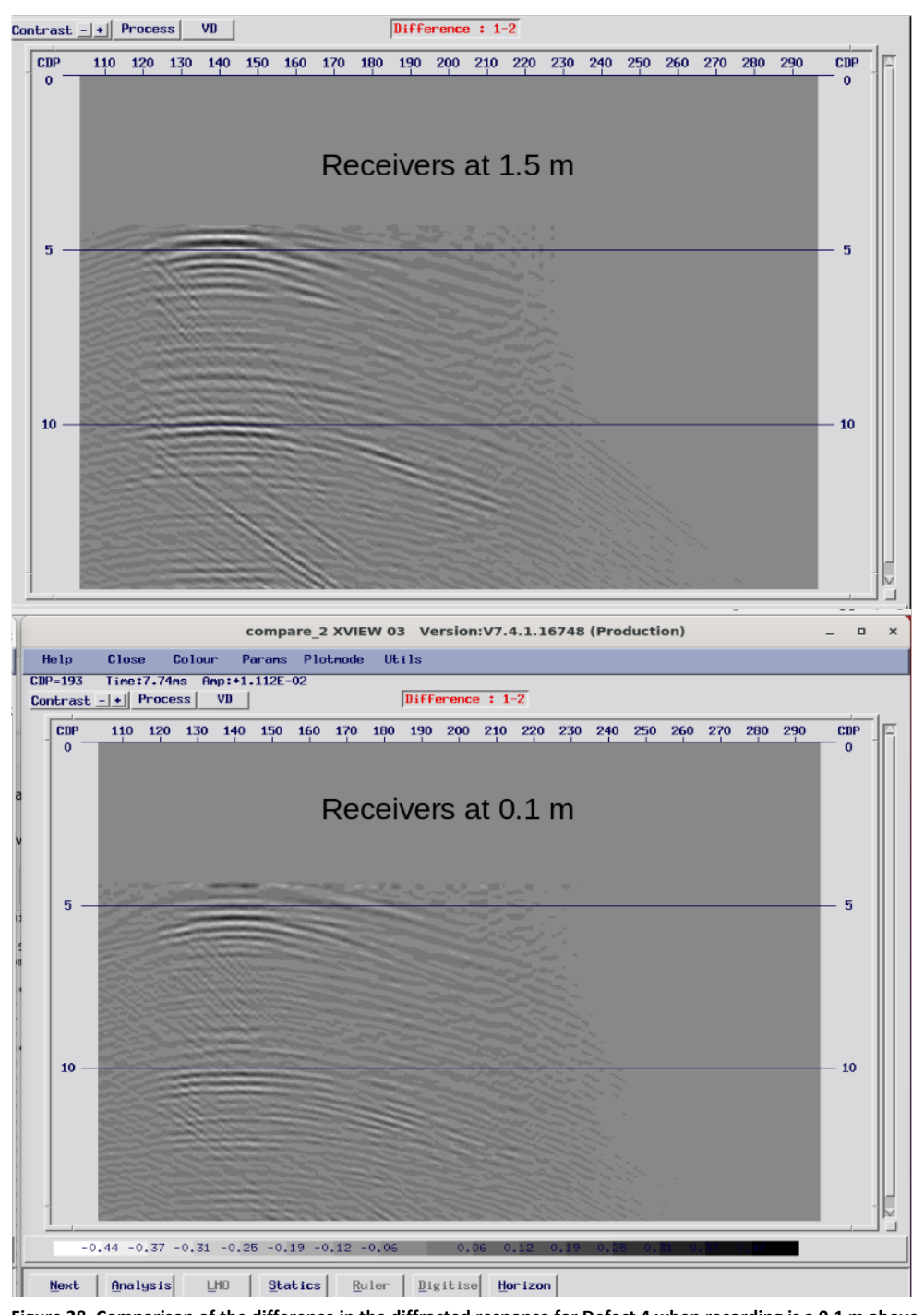


Figure 28. Comparison of the difference in the diffracted response for Defect 4 when recording is a 0.1 m above the base of the dam to when recording is 1.5 m above the base. At the higher level the recording array samples a higher amplitude portion of the diffracted wavefield.

Although it was not possible to image the defects at Älvkarleby it may still be possible to use seismic methods for dam monitoring. We have shown that it is possible to generate the high frequencies required for imaging defects. Theoretically, we can expect to monitor changes in the internal structure of a dam if we can reproduce the source and receiver configurations accurately enough so that we can subtract images from one another from different recording campaigns. Many dams have fiber optic cables already installed for monitoring temperature.



These are fixed in position within the dam and can be used to record acoustic data with an appropriate interrogator (decoder). We propose as a next step to test distributed acoustic sensing (DAS) on a real dam where fiber optic cable(s) are installed. The source used at the experimental dam can be mounted on a fixed rail to increase the repeatability of the source position. The main purpose of such a project would be to verify that the fiber optic cable can be used as a sensor at high frequencies (2000-4000 Hz) and that data recorded have sufficient repeatability from one campaign to the next. In addition, direct information on the internal velocity structure of the dam would be obtained. In some respects, it may be easier to detect defects in a real dam compared to the experimental one. Reflections from the sides and back of the dam interfering with the diffracted signals will be less of a problem. If successful, the employment of the methodology on a larger scale can be considered for long term monitoring.



5 **Conclusions**

Significant operational knowledge was acquired on performing seismic measurements in a dam environment during the eight acquisition campaigns reported on here, in spite of no defects being detected with certainty. The small size of the dam resulted in unwanted signals being generated by the concrete enclosure. These interfered with both diffractions from the defects, but also added complications to velocity determination. It is clear that both the amplitude and frequency content of the recorded signals of interest increased from one campaign measurement to the next. This is attributed to a continuing saturation process within the dam. It is likely that the dam did not reach full saturation, in a "seismic sense", during the course of the measurements.

We have shown that it is possible to generate and record signals with high enough frequency in the dam environment to potentially detect defects. Seismic modeling shows that the diffraction patterns from defects can potentially be detected if timelapse methods can be applied, that is a baseline survey with no defects is subtracted from a survey acquired with defects present. Good repeatability of the recording configuration (sensor location and response) and the source characteristics (location and source function) are required for these methods to be successful. The source employed at Alvkarleby showed good repeatability concerning the source function when shooting in the reservoir, but location repeatability was poorer. In order to advance the use of seismic methods in dam monitoring it is proposed to use the same source under more controlled conditions at a real dam where fiber optic cable(s) are already installed. This would allow testing of the repeatability of a source-receiver system that could be used for timelapse monitoring in a realistic environment. It would also allow parts of the internal velocity structure of the dam to be mapped, and perhaps monitored for changes with time.



6 References

Adamo N., Al-Ansari, Sissakian V. and Laue J. 2020. Geophysical methods and their applications in dam safety monitoring. Journal of Earth Sciences and Geotechnical Engineering, 11(1), 291–345. doi: 10.47260/jesge/1118

Deangeli C., Giani G.P., Chiaia B. and Fantilli A.P. 2009. Dam failures, Chapter 1. In: De Wrachien D. and Mambretti S. (Eds.) Dam-break Problems, Solutions and Case Studies, WIT Press, ISBN 978-1-84564-142-9.

Ikard S.J., Rittgers J., Revil A. and Mooney M.A. 2014. Geophysical investigation of seepage beneath an earthen dam. Groundwater. doi: 10.1111/gwat.12185

Ivandic M. and Juhlin C. 2018. Geophysical modelling for the Vattenfall experimental dam. Uppsala University, Dept. of Earth Sciences, report to Vattenfall.

Kayode O.T., Odukoya A.M., Adagunodo T.A. and Adeniji A.A. 2018. Monitoring of seepages around dams using geophysical methods: a brief review. IOP Conference Series: Earth and Environmental Science, 173. doi: 10.1088/1755-1315/173/1/012026

Kazemeini H., Juhlin C. and Fomel S., 2010. Monitoring CO2 response on surface seismic data; a rock physics and seismic modeling feasibility study at the CO2 sequestration site, Ketzin, Germany. J. Applied Geophysics, 71, 109-124. doi:10.1016/j.jappgeo.2010.05.004

Kim J.-H, Yi M.-J., Song Y., Seol S.J. and Kim K.S. 2007. Application of geophysical methods to the safety analysis of an earth dam. JEEG, 12(2), 221–235.

Lagerlund J., Bernstone C., Viklander P. and Nordström, E., 2022. Embankment Test Dam of Älvkarleby - Description of installed defects and their position. Mendeley Data, V1, doi: 10.17632/k7zrrbxxnb.1

Norstedt U. and Nilsson A. 1997. Internal erosion and ageing in some of the Swedish Earth and Rockfill dams, Q.73, R.20, 307 p. ICOLD Congress, Florence, Italy.

Salas-Romero S., Juhlin C. and Lundberg E., 2021. Seismic investigations at the Vattenfall experimental dam, Älvkarleby, Sweden. SVC Report VKU14135.

Sharma R.P. and Kumar A. 2013. Case histories of earthen dam failures. Seventh International Conference on Case Histories in Geotechnical Engineering, Chicago.

Woolery E.W. 2018. SH-mode seismic reflection imaging of earthfill dams. Engineering, 4, 694–701.

Zimmer M.A., 2003. Seismic velocities in unconsolidated sands: Measurements of pressure, sorting and compaction effects. PhD thesis, Stanford University.



SEISMIC INVESTIGATIONS AT THE VATTENFALL EXPERIMENTAL DAM, ÄLVKARLEBY, SWEDEN: STAGE 2

Even though no defects were detected valuable experience has been gained in applying seismic methods to dam monitoring. As a next step it is suggested that distributed acoustic sensing (DAS) be tested on a real dam where fiber optic cables are already installed to determine if the high frequencies recorded at Älvkarleby can also be recorded on such a sensor. Other objectives would be to better test the repeatability of the source and determine velocities within the real dam by recording along the entire fiber optic layout.

A new step in energy research

The research company Energiforsk initiates, coordinates, and conducts energy research and analyses, as well as communicates knowledge in favor of a robust and sustainable energy system. We are a politically neutral limited company that reinvests our profit in more research. Our owners are industry organisations Swedenergy and the Swedish Gas Association, the Swedish TSO Svenska kraftnät, and the gas and energy company Nordion Energi.

